The Helix−Coil Transition of DNA Duplexes and Hairpins Observed by Multiple Fluorescence Parameters[†]

György Vámosi[‡,§] and Robert M. Clegg*[,‡,||]

Max-Planck-Institut für Biophysikalische Chemie, Abteilung Molekulare Biologie, Am Fassberg 11, D-37077 Göttingen, Germany, Department of Physics and Laboratory for Fluorescence Dynamics, Loomis Laboratory of Physics, 1110 West Green Street, Urbana, Illinois 61801-3080, and Department of Biophysics and Cell Biology, Medical University of Debrecen, H-4012 Debrecen, Hungary

Received November 10, 1997; Revised Manuscript Received June 24, 1998

ABSTRACT: The thermal denaturation of 8−20-bp DNA duplexes labeled with fluorescein and tetramethylrhodamine at opposing 5′-ends was investigated by monitoring the fluorescence intensity of the dyes, the fluorescence anisotropy of tetramethylrhodamine, the fluorescence resonance energy transfer between fluorescein and rhodamine, and, for the 20-bp duplex, the UV absorption. Melting experiments with the single strands of the duplexes revealed that the single strands can form hairpins stabilized by only a few base pairs. The thermal denaturation curves of the duplexes were fitted well to an extended all-or-none model assuming that only the fully base-paired duplex, the maximally base-paired hairpin, and the random coil conformations are present simultaneously. The extent-of-melting versus temperature curves derived from the different spectroscopic parameters are nearly identical, provided that the analysis of the baselines is carried out correctly; the ΔH and ΔS of the dissociation compare well with predictions based on nearest neighbor interaction values available in the literature. Our results imply that for all the oligonucleotides other than the 34-bp oligomer, no partially melted intermediates other than hairpins are present in the reaction mixture in amounts that can be detected by our methods. The melting of the hairpins was also studied directly using single-stranded oligonucleotides. The melting of a 34-bp duplex can be accounted for by a statistical zipper model.

It is now routinely possible to synthesize oligonucleotides of any desired sequence and label them site-specifically with one or more fluorophores. We and others have used fluorescence spectroscopic measurements, especially Förster-type fluorescence resonance energy transfer (FRET), to determine the structures of nucleic acid molecules. The helical geometry of DNA[1] in solution has been observed by FRET using duplexes labeled with fluorescein and TMRh (*1*). The structures of bulged DNA and RNA molecules (*2*) and three- and four-way branched DNA molecules (*3*−*9*) were determined using similar methods. Fluorescence methods are also sensitive tools for investigating conformational changes such as the helix−coil transition of nucleic acid molecules (*1, 10*−*14*). The fluorescence of a dye is sensitive to the surrounding environment, and it is a sensitive indicator of the conformation of an oligonucleotide to which it is attached. The different fluorescence parameters, such as the intensity, anisotropy, lifetimes, spectra, and FRET, reveal different aspects of the molecular structures, and this can help elucidate the molecular mechanism of nucleic acid thermal denaturation. It is advantageous to measure as many spectroscopic parameters as possible in order to extract a detailed description of the strand-dissociation reaction and to avoid overlooking processes that may remain hidden when monitoring a single spectroscopic parameter. The investigation of relatively simple linear duplexes and their single-stranded counterparts is important in order to be able to interpret results obtained with more complex structures, such as branched molecules and bulged duplexes.

The thermal denaturation of very short oligomers is often described by a two-state all-or-none model, which assumes that only the completely intact bimolecular duplex structure and the completely melted random coil can be discerned in the reaction mixture. This approximation becomes less valid as the chain length of the oligomer increases because larger fractions of the molecules exist in partially melted intermediate states during the course of the melting process. In addition, other conformations, such as hairpin structures, can be present. Such intermediates might be observed by a multiparameter analysis of fluorescence data. The different spectroscopic parameters might be sensitive to different molecular events in the series of steps toward the complete dissociation of the duplex. If so, the temperature profiles of the extent-of-melting curves could depend on which fluorescence parameter is used to monitor the denaturation; in this case, the data must be correctly analyzed in order to determine accurate thermodynamic parameters describing the

[†] G.V. and R.M.C. thank the Deutsche Forschungs Gemeinschaft for financial support: DFG-Project Nr. II B 2 C1 84/2-2.

* Author to whom correspondence should be addressed. E-mail: clegg@physics.uiuc.edu.

[‡] Max-Plank-Institute für Biophysikalische Chemie.

[§] Medical University of Debrecen.

[||] Loomis Laboratory of Physics.

[1] Abbreviations: bp, base-pair; DNA, deoxyribonucleic acid; ds, double-stranded; ss, single-stranded; hp, hairpin; rc, random coil; TMRh, tetramethylrhodamine; ΔH, molar enthalpy change; ΔS, molar entropy change; ΔG, molar Gibbs free energy change.

S0006-2960(97)02760-8 CCC: $15.00
Published on Web 09/12/1998

stabilization of the duplex structure, and to compare the experimentally determined thermodynamic parameters derived from the different spectroscopic measurements with the thermodynamic parameters available in the literature (*15*). A treatise of helix−coil transition theories and experiments for polypeptides and nucleic acids, with an extensive collection of original papers, is available (*16*).

We have shown previously by time-resolved decay parameters and steady-state measurements of TMRh fluorescence (*17*) that in the double-stranded form the TMRh−DNA complex can exist in three major conformations: two fluorescent species with lifetimes of ∼1 ns and ∼3−4 ns, and a "dark" species (this isomeric form of the TMRh−DNA complex has a very low quantum yield; that is, a very short lifetime). Species with similar photophysical characteristics are also present in the single-stranded form, but with less, or no, contribution from the "dark" state. In addition, the TMRh−DNA complex in the double-stranded form appears to interact with two Na^+ ions that hinder the rotation of the TMRh molecule. The temperature dependence of the fluorescence parameters in the pure double- or single-stranded forms, that is, the shape of the baselines of the fluorescence melting curves, is determined by the temperature-dependent redistribution of TMRh between the different conformations. Knowledge of the spectroscopic and thermodynamic characteristics of these different conformations is crucial for making a correct analysis of the fluorescence melting curves. We show here that reliable quantitative analyses of the fluorescence melting curves require a knowledge of the photophysical characteristics of the dyes and of the particular spectroscopic parameter.

In this work, we have measured the temperature dependencies of the steady-state fluorescence intensity and the steady-state anisotropy of the fluorescein and tetramethylrhodamine attached to the 5′-end of single- and double-stranded oligonucleotides, and the efficiency of FRET between the two fluorophores in doubly labeled molecules. The fluorescence intensity provides information about the conformation of the macromolecule in the vicinity of the dye (*17*). Fluorescence anisotropy reports on the local as well as the overall rotational mobility of the dye and the dye−DNA complex. FRET between two dyes attached at different positions of the macromolecule reports on the relative spatial and angular disposition of the two chromophores.

The experiments showed that the single-stranded molecules are not always in a random-coil state; for instance, the single strands can exist as hairpins, as well as having a completely non-base-paired conformation. The thermal denaturation curves of the duplexes are influenced by the formation of hairpins of the single-stranded oligonucleotides; the presence of a hairpin conformation influences the spectroscopic parameters of the dyes near the hairpin structure, as well as the thermodynamics of the main duplex−random coil transition. During the thermal denaturation process the duplex, hairpin, and random coil species are simultaneously present. Measurement of different spectroscopic parameters made it possible to deconvolve the dissociation of the strands from the melting curves. Similar equilibria of the duplex and hairpin DNA (*18, 19*) and duplex, hairpin, and random coil conformations (*20*−*24*) have been observed by NMR studies of oligonucleotides; such measurements require sample concentrations many orders of magnitude higher than those used in this study. A review on the structural and thermodynamic aspects of stable nucleic acid hairpins and their biological function has recently been published (*25*).

MATERIALS AND METHODS

Construction of Fluorescently Labeled Single- and Double-Stranded DNA Oligonucleotides. The synthesis, purification, labeling, and hybridization of single-stranded (ss), hairpin (hp), and double-stranded (ds) oligonucleotides (*17*) are described in detail in previous studies. The main steps of the procedures are as follows. Oligonucleotides were synthesized on an Applied Biosystems 392 DNA/RNA synthesizer with β-cyanoethylphosphoramidite chemistry (*26*). In the final step of the synthesis amino groups at the end of six-carbon linkers were coupled to the 5′-end of the DNA strands with *N*-methoxytrityl-2-aminohexyl-2-cyanoethyl-*N*,*N*-diisopropyl aminophosphite (*27*). Sequences of the "top strands" of duplexes were the following: 8-base, 5′-CCACTAGG-3′; 12-base, 5′-CCACTGGCTAGG-3′; 16-base, 5′-CCACTGCACTGCTAGG-3′; 20-base, 5′-CCACTGCACTCGCTGCTAGG-3′; and 34-base, 5′-CCAGACTGCAGTTGAGTCCTTGCTAGGACGGAGG-3′. Two other single strands, an 8-base, 5′-CCACTACC-3′, and a 16-base, 5′-CCACTGCACTGCTACC-3′, were synthesized. These last two single-stranded probes have CC at the 3′-end instead of GG to avoid the formation of hairpins in the single-stranded state. Oligonucleotides were purified with anionic exchange and reverse-phase HPLC. Fluorescence labeling was carried out at the 5′ amino groups of the strands with 5-carboxytetramethylrhodamine *N*-hydroxysuccinimide ester and of the complementary strands with 5-carboxyfluorescein isothiocyanate (Molecular Probes, Eugene, OR) in 0.2 and 0.3 M carbonate buffer at pH 9.5. The stock solutions of the dyes were originally dissolved in dry dimethylformamide or dimethylsulfoxide. Unreacted dyes were removed by chromatography on Sephadex G25 columns (Pharmacia, Uppsala). Labeled oligonucleotides were purified by polyacrylamide gel electrophoresis (PAGE) on 20% gels. Complementary sequences were hybridized to form duplex molecules in 450 mM NaCl/24 mM sodium citrate/2 mM $MgCl_2$ at pH 7.0 by slow cooling from 80 to 0 °C (the water bath was brought to 80 °C, then the bath was turned off and slowly cooled to room temperature; then the sample was cooled slowly to 0 °C). Double-stranded molecules were constructed with one fluorescein label only, with one rhodamine label only, and with one fluorescein and one TMRh label at opposing ends of the duplexes. The 34-bp duplex was labeled only with TMRh. The single strands labeled with TMRh were also used in melting experiments. The duplex molecules were purified by PAGE on 10−20% gels. Labeled duplexes were extracted from the gel slices by electro-elution or by soaking in buffer at 4 °C for the shorter molecules. Double- and single-stranded molecules were dissolved in 10 mM sodium phosphate pH 7.46, 80 mM NaCl. The buffer was prepared by mixing Na_2HPO_4 and NaH_2PO_4. At pH 7.46 the Na^+ concentration of this phosphate buffer is 18 mM. Phosphate buffer was chosen because its pH is essentially temperature-independent. The experiments with the 34-bp duplex and the 12-bp single strands were carried out in a different buffer containing 68 mM tris-borate, 76 mM NaCl, 0.076 mM EDTA, and 30 wt

% glycerol. The extent of labeling and the concentration of the duplexes were calculated from absorption spectra taken from 220 to 600 nm. For the determination of the concentration of the duplexes a molar extinction value of $\epsilon_{260nm} = 13\,000\ M^{-1}\ cm^{-1}\ bp^{-1}$ was used.

The Thermal Denaturation of DNA Molecules. The melting process was monitored by measuring several different fluorescence parameters and UV absorption. The temperature change was precise within ±0.1 °C; the step size (1−3 °C steps) depended on the range of the transition being measured; the step size was small around the T_m and greater in the pre- and post-melting regions. The temperature in the cuvette was set by a water-jacketed cuvette holder connected to a water bath; the temperature was measured in a second water-jacketed cuvette by a thermistor. DNA molecules were denatured in a discontinuous heating process. The temperature change in the cuvette was complete within 5 min; 10 min was then allowed for equilibration of the reaction components before taking the fluorescence and absorption measurements. For absorption measurements the temperature was controlled by a computer; for the fluorescence measurements the bath was controlled manually.

Spectroscopy Equipment. The absorption measurements were taken on a Uvicon 820 (Kontron, Zürich) spectrophotometer; the absorption of the buffer was always subtracted. For melting curves the absorption spectra were measured from 240 to 274 nm in 2 nm steps, and the absorption values in this wavelength range were averaged in order to improve the signal-to-noise ratio. Fluorescence measurements were made on an SLM 8000S (SLM Aminco, Urbana, IL) spectrofluorimeter with a cooled photomultiplier; the data were acquired in the single-photon counting mode. All fluorescence data were corrected for fluctuations in the lamp intensity. Polarization artifacts of the emission spectra were circumvented by using magic angle conditions between excitation and emission polarizers (*28*). Emission spectra were corrected for wavelength variations of the detection efficiency of the instrument. Excitation slits were set at 4 nm and emission slits at 2, 4, or 8 nm depending on the fluorescence intensity of the sample. Emission spectra were taken over broad wavelength ranges: $\lambda_{ex} = 490$ nm (which excites fluorescein and to a small extent TMRh), $\lambda_{em} = 500-650$ nm and $\lambda_{ex} = 560$ nm (for exciting TMRh alone), and $\lambda_{em} = 570-650$ nm. From these spectra a parameter called "$(ratio)_A$", which is linearly dependent on the efficiency of FRET between the fluorescein and TMRh labels, was determined for doubly labeled duplexes (see below). Steady-state anisotropy was measured in the L configuration at two different excitation−emission wavelength pairs: $\lambda_{ex} = 490$ nm and $\lambda_{em} = 518$ nm for fluorescein, and $\lambda_{ex} = 560$ nm and $\lambda_{em} = 590$ nm for TMRh. Steady-state fluorescence intensity of the two dyes was measured at the same excitation and emission wavelengths as the anisotropy.

Measuring Fluorescence Lifetimes of TMRh. Nanosecond lifetime measurements were carried out with the phase and modulation method (*29, 30*) The instrumentation differs only slightly from that described in ref *31*. See ref *17* for details. Phase and modulation data were acquired at 13 excitation frequencies ranging from 1 to 140 MHz and analyzed with a software package from Globals Unlimited (Laboratory for Fluorescence Dynamics, Urbana, IL). This program yielded the τ_i fluorescence lifetimes and the α_i contributions of the lifetime components to the steady-state fluorescence intensity. From these data the molecular fractions, a_i, of the lifetime components were determined. The mean fluorescence lifetime for two components which is weighted according to the molecular species is directly proportional to the steady-state fluorescence intensity; it is defined as

$$\langle\tau\rangle = a_1\tau_1 + a_2\tau_2 \quad (1)$$

The mean lifetimes could be reproduced within ±0.15 ns.

DATA ANALYSES

Calculating Steady-State Fluorescence Anisotropy. Fluorescence anisotropy (r) was calculated from the fluorescence intensities measured at different polarizer settings according to the following equation:

$$r = \frac{F_{vv} - RF_{vh}}{F_{vv} + 2RF_{vh}}, \quad R = \frac{F_{hv}}{F_{hh}} \quad (2)$$

where F_{vv}, F_{vh}, F_{hv}, and F_{hh} are the fluorescence intensities measured at different excitation and emission polarizer settings; the first index refers to the vertical/horizontal setting of the excitation polarizer and the second to the emission polarizer. Background values arising from light scattering of the buffer solution and the dark current of the photomultiplier were subtracted from the corresponding fluorescence intensity values. The correction factor R accounts for the different transmission and detection efficiency of the detection system for the vertically and horizontally polarized light and is constant for a given emission wavelength and slit width setting of the instrument. The denominator of the expression of the anisotropy is proportional to the total fluorescence intensity.

Analyzing FRET. Förster-type fluorescence resonance energy transfer (FRET) is a nonradiative deactivation process where the excitation energy of an excited fluorophore (donor) is transferred to another chromophore (acceptor) through resonance coupling of the emission dipole of the donor with the absorption dipole of the acceptor. It requires the appropriate relative orientation of the dipole moments of the dyes and an overlap between the emission spectrum of the donor and the absorption spectrum of the acceptor (*32, 33*). The rate of the process is directly proportional to the negative sixth power of the distance between the fluorophores. The efficiency E of FRET is the fraction of excited donor molecules that transfer their excitation energy to acceptor molecules and it is equal to

$$E = \frac{k_T}{\sum_i k_i} = \frac{1}{1 + (R/R_0)^6},$$

$$R_0^{\,6} = (8.79 \times 10^{-28}\ mol)(n^{-4}Q_d\kappa^2 J) \quad (3)$$

where K_T is the rate constant of the energy transfer, $\sum_i k_i$ is the sum of the rate constants of all deactivation processes including those of fluorescence and FRET, R is the distance between the acceptor and the donor, R_0 is the Förster critical distance for which $E = {}^1/_2$, n is the index of refraction of the medium between the dyes, Q_d is the fluorescence quantum yield of the donor in the absence of the acceptor,

κ^2 is an orientation factor (often approximated by $^2/_3$ which is often a good estimate if at least one of the dyes has a dynamically randomized orientation (*34*, *35*)), and J is the overlap integral of the fluorescence emission and absorption spectra of the donor and the acceptor, respectively. R_0 for DNA duplexes labeled with fluorescein as the donor and TMRh as the acceptor was estimated to be 45 Å (*1*) or 50−60 Å (*2*); this depends on the particular isomers used for the labeling, on the temperature due to the temperature-dependent distribution of the TMRh among the different TMRh−DNA complexes (*17*), and on the quantum yield of fluorescein. The efficiency of FRET was determined from $(\text{ratio})_A$ (*4*), which is a normalized measure of the enhancement of the fluorescence from the acceptor due to FRET,

$$(\text{ratio})_A = \frac{F^{A(D)}(490,\lambda)}{F^{A(D)}(560,\lambda)} = \frac{[\epsilon^D(490)E + \epsilon^A(490)]\phi^A(\lambda)}{\epsilon^A(560)\phi^A(\lambda)} = \frac{\epsilon^D(490)}{\epsilon^A(560)}E + \frac{\epsilon^A(490)}{\epsilon^A(560)} \quad (4)$$

where $F^{A(D)}(490,\lambda)$ is the fluorescence intensity of the acceptor (only the acceptor fluorescence) in the presence of the donor measured at the emission wavelength λ if the sample is excited at 490 nm, $F^{A(D)}(560,\lambda)$ is the intensity of the acceptor excited at 560 nm, ϵ^D and ϵ^A are the molar absorption coefficients of the donor and the acceptor at the indicated wavelengths, and $\phi^A(\lambda)$ is a shape function of the acceptor emission spectrum. The numerator of the expression is the sum of the emission of the acceptor due to FRET and direct excitation (both spectra excited at 490 nm), while the denominator is the fluorescence of the acceptor due to direct excitation at 560 nm. $F^{A(D)}(490,\lambda)$ can be calculated by measuring the total emission of the doubly labeled molecule excited at 490 nm and subtracting the contribution of the donor emission from it (*4*). Specifically the calculation of $(\text{ratio})_A$ was performed by fitting the fluorescence emission spectrum ($\lambda_{ex} = 490$ nm, $\lambda_{em} = 500-650$ nm) of the doubly labeled duplex to a linear combination of the emission spectra of a donor-labeled molecule ($\lambda_{ex} = 490$ nm, $\lambda_{em} = 500-650$ nm) and of the doubly labeled molecule ($\lambda_{ex} = 560$ nm, $\lambda_{em} = 570-650$ nm). The best-fit coefficient of the latter spectrum in the linear combination is equal to $(\text{ratio})_A$. The fitting procedure was written in the program LabVIEW (National Instruments, Austin) implemented on a Macintosh computer by R. M. Clegg and C. Gohlke. The parameter $(\text{ratio})_A$ is a linear function of the FRET efficiency, and its temperature dependence can be used to determine the extent-of-melting (see below).

Fitting the Temperature Profiles of the Different Spectroscopic Parameters According to Different Thermodynamic Models. The temperature dependence of the fluorescence intensity of both dyes, the anisotropy of TMRh, $(\text{ratio})_A$, and UV absorption curves were analyzed by means of nonlinear fitting techniques in order to determine the ΔH and ΔS (molar enthalpy and entropy changes) of the helix−coil transition, and the fraction $\alpha(T)$ of melted molecules, that is, the extent-of-melting. The spectroscopic observables were expressed as a function of the temperature and the fit parameters; the variance between the fit and the experimental data was minimized in iterative steps using the program IGOR Pro (WaveMetrics, Lake Oswego, OR) run on a Power Macintosh computer. For the 8−20-bp duplexes the parameters that define the baselines (see below for the models used to approximate the baselines) were determined simultaneously with the thermodynamic parameters during the fitting procedure. The temperature-dependent values of α that appear in the expressions for the spectroscopic observables (see next section) were expressed in terms of the appropriate thermodynamic parameters of the equilibrium equations of the helix−coil transition (see Appendix eqs A-3−6). The melting of the hairpins was described with a monomolecular all-or-none model (see eq A-4). For the melting of the 8-, 12-, 16- and 20-bp duplexes, an extended all-or-none model was used assuming the presence of three species: fully base-paired duplex, one species of hairpin, and random coil single-stranded molecules (see eqs A-5,6). The dissociation of the 34-bp duplex was described by a simple all-or-none model (see eq A-3) assuming duplex and single-strand conformations (no hairpin); the melting of this molecule was also simulated with a statistical zipper model (see eqs A-9−12), taking into account intermediate states. A detailed description of the different thermodynamic and statistical models and the corresponding equilibrium equations of the helix−coil transition are given in the Appendix.

Dependence of the Spectroscopic Parameters on the Extent-of-Melting. The observed parameters can be divided into two groups depending on how the extent-of-melting (α) affects the value of the spectroscopic parameter. The fluorescence intensity and the UV absorption depend linearly on α

$$F = (1 - \alpha)F_{ds} + \alpha F_{ss} \quad (5)$$

where F is the molar fluorescence intensity of the ds-ss mixture, F_{ds} and F_{ss} are the baselines, that is, the molar fluorescence intensities of the pure ds and pure ss species. A similar expression holds for UV absorption melting curves. Note that F_{ds} and F_{ss} can be temperature-dependent.

The anisotropy, r, and the $(\text{ratio})_A$ values of the reaction mixture depend on α in a nonlinear fashion because α is present both in the numerator and in the denominator of the expression

$$r = \frac{(1 - \alpha)F_{ds}r_{ds} + \alpha F_{ss}r_{ss}}{(1 - \alpha)F_{ds} + \alpha F_{ss}},$$

$$(\text{ratio})_A = \frac{(1 - \alpha)F_{ds}(\text{ratio})_{A,ds} + \alpha F_{ss}(\text{ratio})_{A,ss}}{(1 - \alpha)F_{ds} + \alpha F_{ss}} \quad (6)$$

where r_{ds}, r_{ss}, $(\text{ratio})_{A,ds}$, and $(\text{ratio})_{A,ss}$ are the double- and single-strand baselines of the corresponding parameters. The derivation of eq 6 for the expression of $(\text{ratio})_A$ is given in the Appendix.

The Baselines of the Melting Curves of Duplexes. The baselines are the temperature-dependent curves of the pure double-stranded and single-stranded species of the spectroscopic parameters. The baselines of the absorption melting curves in the ds and the ss states were approximated by straight lines, as were the baselines of the fluorescence intensity of fluorescein. The nonlinear double-strand baseline of TMRh fluorescence, F_{ds}, was fitted according to a simple monomolecular transition between two fluorescent states with differing molar fluorescence intensities. The single-strand

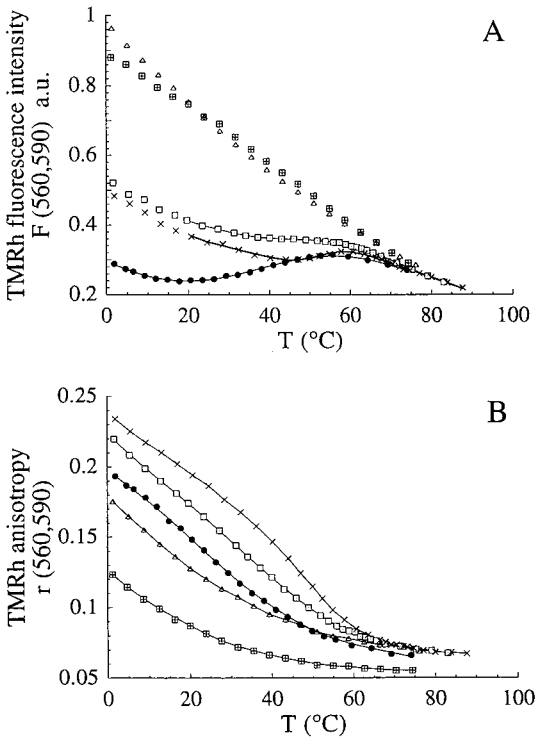

FIGURE 1: Temperature dependence of the fluorescence parameters of the TMRh-labeled strands. Original sequences: 8-base hairpin (●), 16-base hairpin (⊡), and 20-base hairpin (×). Modified sequences: 8-base random coil (⊞) and 16-base random coil (△). Exchanging the original GG bases for CC at the 3′-end of the DNA strand prevents hairpin formation and base pairing between the bases at the 3′-end and the CC bases at the 5′-end. The buffer contained 10 mM sodium phosphate, pH 7.4, and 80 mM NaCl. (A) Fluorescence intensity (exc., 560 nm; em., 590 nm) of TMRh. The solid lines are nonlinear fits corresponding to a monomolecular reaction representing the melting of the hairpin structure (see eq A-4 of the Appendix). The baselines were fitted to straight lines. (B) Fluorescence anisotropy of TMRh. The solid lines are not theoretical fits.

fluorescence baseline, F_{ss}, was determined from experiments with the TMRh-labeled strand of the 8-, 16-, 20-, and 34-base molecules; the 12-base baseline was fitted with a straight line because the 12-base single-strand melting curve was taken in a different buffer than the duplex. The $(\text{ratio})_{A,ds}$ and $(\text{ratio})_{A,ss}$ baselines were also approximated by straight lines. The temperature dependence of F_{ds} and F_{ss} in the expressions for $(\text{ratio})_A$ and r was taken over from the fluorescence intensity fits. The ds baseline r_{ds} of the TMRh anisotropy was fitted to a straight line, whereas the single-strand baseline r_{ss} was determined experimentally with the TMRh-labeled strand (except for the 12-base where r_{ss} of the 16-base strand plus a constant were fitted to the experimental data).

RESULTS

Fluorescence Intensity and Anisotropy of the TMRh-Labeled DNA Single Strands. The temperature profiles of the fluorescence intensity and anisotropy for the 8-, 16-, and 20-base TMRh-labeled single strands are shown in Figure 1. The 12-base single-strand melting curve is not shown, because it was measured in a different buffer solution than the other molecules (see Materials and Methods). The van't Hoff enthalpies and entropies derived from the fits are shown in Table 1. We also measured the fluorescence intensity and anisotropy melting curves of the TMRh-labeled 8- and 16-base strands with modified sequences. In these molecules the GG bases at the 3′-end were changed for CC in order to avoid the formation of hairpins.

Table 1: The Thermodynamic Parameters of the Melting of the Hairpins[a]

sample	ΔH (kcal/mol)	ΔS (cal/mol/K)	ΔG (kcal/mol)	T_m (°C)
8-base strand	17.0 ± 5	54.3 ± 16	0.8	40.0 ± 6
16-base strand	28.0 ± 7	87.0 ± 22	2.1	48.2 ± 5
20-base strand	58.5 ± 10	179.3 ± 32	5.0	53.1 ± 2
12-base strand[b]	22.0 ± 5	70.7 ± 16	0.9	37.9 ± 5

[a] The values of ΔH and ΔS, the molar enthalpy and entropy changes of the melting of the hairpin structures, were determined from nonlinear fits of the fluorescence intensity versus temperature curves of the TMRh-labeled single strands shown in Figure 1A. The buffer solution of the 8-, 16-, and 20-base strands contained 10 mM sodium phosphate, pH 7.46, and 80 mM NaCl. The Gibbs free energy, $\Delta G = \Delta H - T\Delta S$, was calculated from ΔH and ΔS at $T = 25$ °C. [b] The buffer solution for the 12-base hairpin was different than for the other molecules; it contained 68 mM tris-borate, 76 mM NaCl, 0.076 mM EDTA, and 30 wt % glycerol.

Fluorescence Melting Curves of the 8-, 12-, 16-, 20-, and 34-bp Duplexes. Monitoring the Melting of the 8−20-bp Duplexes by Multiple Fluorescence Parameters and Analyzing the Melting Process According to the Extended All-or-None Model. Panels A−F of Figure 2 show the temperature profiles of the different spectroscopic parameters (fluorescence intensity, anisotropy, energy transfer, and mean lifetime) of the 8-, 12-, 16-, and 20-bp duplexes.

Fluorescence Intensity of TMRh and Fluorescein. The fluorescence intensities of 8-, 12-, 16-, and 20-bp duplexes labeled with TMRh are presented as a function of temperature in Figure 2A. The lower baselines (due to the double-stranded state) were approximated by a monomolecular equilibrium between two states with different molar fluorescence intensities (*17*). The temperature-dependent fluorescence curves of the hairpin molecules were used as single-strand baselines (except for the 12-base molecule where the single-strand baseline was fitted to a straight line because the buffer of the single-stranded sample was different than that of the other samples, and such the data could not be used for the duplexes). Figure 2B shows the fluorescence intensity versus temperature curves of the fluorescein label for the doubly labeled duplexes. The baselines of these curves were fitted to straight lines.

Fluorescence Anisotropy of TMRh and Fluorescein. The fluorescence anisotropy of TMRh of the doubly labeled 8−20-bp duplexes is shown in Figure 2C. The anisotropy melting curves were fitted according to eq 6. The double-strand baselines of the TMRh anisotropy curves were fitted to straight lines, and the anisotropy melting curves of the hairpin molecules were used as the single-strand baselines.

The anisotropy of the fluorescein label of the doubly labeled duplexes is shown in Figure 2E. The temperature dependence of the anisotropy curves of the fluorescein label was not analyzed thermodynamically.

FRET Melting Curves. The efficiency of energy transfer of the doubly labeled duplexes was monitored by the parameter $(\text{ratio})_A$. The melting curves monitored by $(\text{ratio})_A$ are shown in Figure 2D. $(\text{ratio})_A$ is linearly dependent on

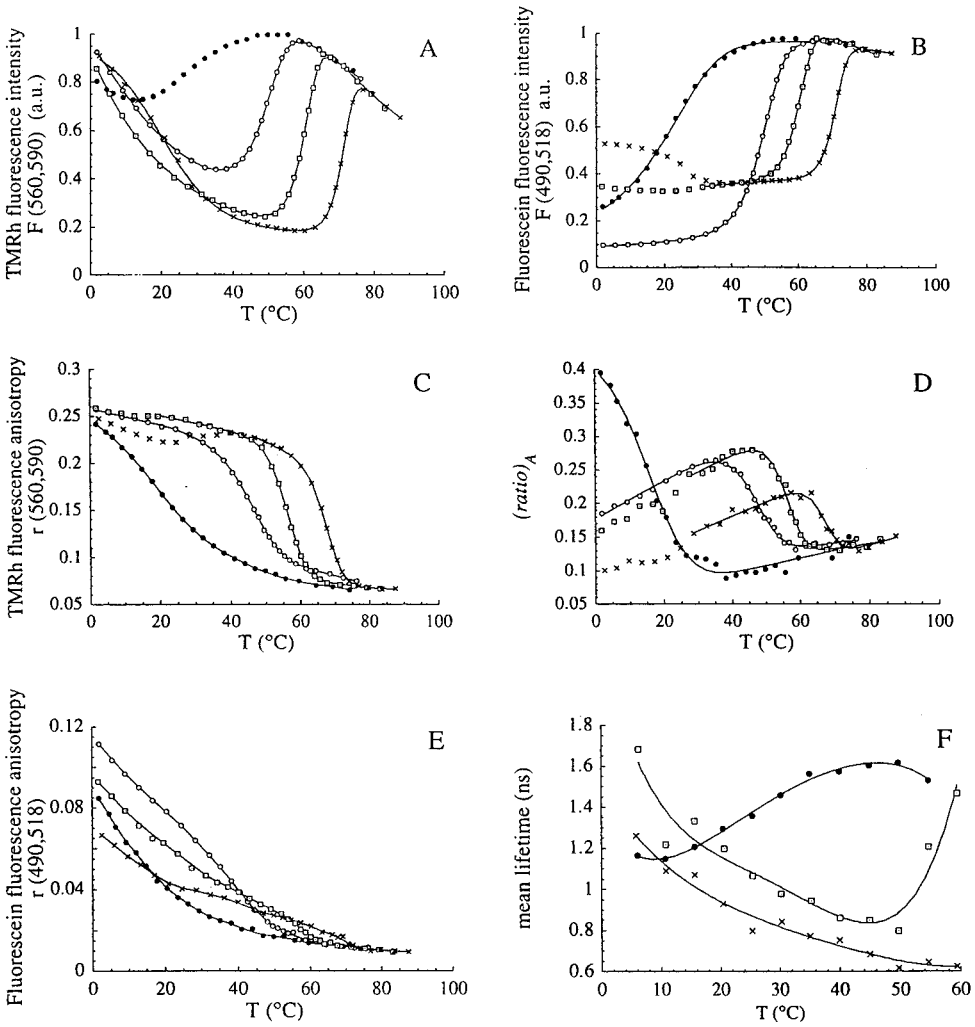

FIGURE 2: Temperature dependence of the different fluorescence parameters measured on the duplexes. Duplex lengths: 8 bp (●), 12 bp (○), 16 bp (⊡), and 20 bp (×). Unless otherwise indicated, the solid lines represent fits according to an extended model including three states: a fully base-paired duplex, one hairpin molecular species and a non-base-paired random coil. For the model equations see eqs A-5 and A-6, and for the connection between the extent-of-melting and the spectroscopic parameter see eqs 5 and 6. The concentrations of the samples are all in the range of 300−400 nM. The duplexes used in the measurements were doubly labeled with fluorescein and TMRh, except for the lifetime measurements, where they were singly labeled with TMRh. The buffer contained 10 mM sodium phosphate, pH 7.4, and 80 mM NaCl. (A) Fluorescence intensity of the TMRh label (exc., 560 nm; em., 590 nm). Intensities were normalized to one another in the high-temperature range, where all molecules are supposedly in the single-stranded form; the maximum was arbitrarily set to 1. (B) Fluorescence intensity of the fluorescein label (exc., 490 nm; em., 518 nm), normalized as above. (C) Fluorescence anisotropy of the TMRh label (exc., 560 nm; em., 590 nm). (D) $(\text{Ratio})_A$, the normalized acceptor emission, a parameter depending linearly on the efficiency of FRET. (E) Fluorescence anisotropy of the fluorescein label (exc., 490 nm; em., 518 nm). Solid lines are not theoretical fits. (F) Mean lifetime (see text) of the TMRh label of the 8-, 16-, and 20-bp duplexes. Solid lines are not theoretical fits.

E. The temperature-dependent $(\text{ratio})_A$ curve was fitted according to eq 6. The baselines of these curves were approximated by straight lines.

Melting Curves of the 34-bp Duplex. The fluorescence intensity melting curve of the TMRh-labeled 34-bp duplex is shown in Figure 3A. Measurements with the labeled single strands indicate that it is probable that the single strand can form a hairpin (data not shown); however, the T_m of this hairpin is far below the T_m of the duplex and the two melting processes do not appreciably overlap. The data were fitted with a simple all-or-none model involving duplex and single-stranded (random coil) conformations (see eq A-3 of the Appendix). The double-strand baseline was fitted to a monomolecular equilibrium between two states of the TMRh−DNA complex. The temperature dependence of the fluorescence intensity of the TMRh-labeled single strand was measured, and this curve was used as the single-strand baseline. The result of the all-or-none fit to the duplex melting curve is shown in Figure 3A.

The melting process of the 34-bp duplex was also simulated with the statistical zipper model. A model-independent extent-of-melting curve was calculated by fitting the duplex and single-strand baselines, F_{ds} and F_{ss}, in the double- and single-stranded regions, and then calculating $\alpha(T) = [F(T) - F_{ds}(T)]/[F_{ss}(T) - F_{ds}(T)]$. The $\alpha(T)$ curves were then fitted to the zipper model by allowing the average enthalpy change, corresponding to the opening of a base-pair $\langle \Delta H_{bp} \rangle$, to vary while holding other parameters constant at different values; simulated curves from such fits are shown in Figure 3B. The position of the base pairs that influence the fluorescence signal was varied. The zipper model fits the experimental curve best if the assumption is made that the base pairs 1−5, 2−5, or 3−5 at the TMRh-labeled end of the molecule influence the fluorescence intensity signal.

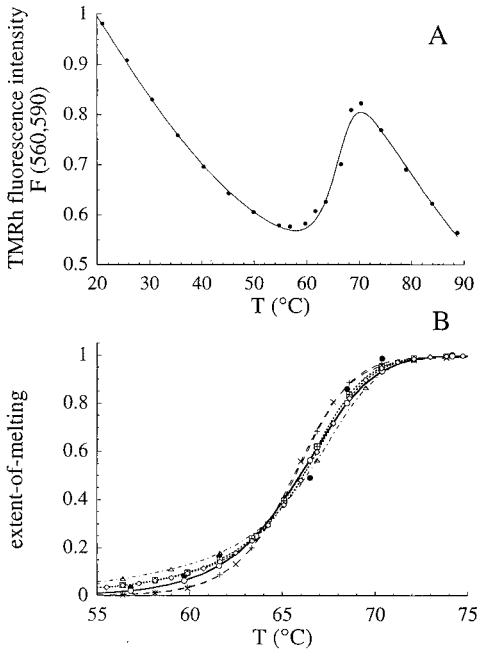

FIGURE 3: The melting of the 34-bp duplex. (A) Fluorescence intensity of TMRh (exc., 560 nm; em., 590 nm). The solid line is a two-state fit. The concentration of the sample was ~10 nM, and the buffer contained 68 mM tris borate, 76 mM NaCl, 0.076 mM EDTA, and 30 wt % glycerol. (B) Extent-of-melting curves: experimental data (●), two-state fit (○), and five simulations according to the statistical zipper model. The two-state fit deviates considerably from the experimental curve both in the low- and high-temperature region of the melting and yields $\Delta H = 194$ kcal/mol which is 76% of the value predicted by a nearest-neighbor calculation based on ref *15*. The four other curves represent simulations according to the zipper model, assuming that the helix or coil state of the last "*n*" bases affects the fluorescence signal, n being 4 (△), 5 (⊞), 10 (+), and 34 (×); the diamond (◇) represents a simulation when the third, fourth, and fifth base pairs counted from the end affect the signal. The average ΔH due to the helix-to-coil transition of a single base pair was varied to find the best-fitting curve allowed by the model in the range of 8.28−8.34 kcal/mol/bp, while ΔS was set to 24 cal/mol/K. The simulations with $n = 5$ (⊞) or that observing bases 3−5 (◇) are closest to the experimental curve and give better agreement with the data than the two-state fit. The simulated curves for $n = 10$ and 34 are almost identical.

The $\langle \Delta H_{bp} \rangle$ values yielding the best fit to the experimental data are given in the legend of Figure 3B. The average entropy change $\langle \Delta S_{bp} \rangle$ was set to 24 cal/mol/K.

Enthalpy and Entropy Changes of the Helix−Coil Transition. Extent-of-Melting Curves Obtained from the Different Parameters. The nonlinear fits according to the extended all-or-none model (see Appendix) of the fluorescence melting curves of the doubly labeled 8−20-bp duplexes and the UV absorption melting curves of the 20-bp duplex labeled with TMRh yielded the enthalpy (ΔH) and entropy (ΔS) changes of the denaturation process and the parameters defining the baselines. The thermodynamic model and the baselines were fitted simultaneously. By using the best-fit parameters we calculated the extent-of-melting (α) curves (see Figure 4). For these molecules α is the molecular fraction of all single-stranded molecules, that is, the total fraction of hairpin and random coil conformations. The ΔH and ΔS values for melting are presented in Table 2. These values represent the enthalpy and entropy differences between the duplex and random coil states. The enthalpy changes are also shown in Figure 5. The enthalpy values estimated using the nearest neighbor ΔH and ΔS values from ref *15* are also given in Table 2. The concentration of the TMRh-labeled 20-bp duplex (1 μM) used in the melting experiment monitoring UV absorption and that of the doubly labeled 20-bp duplex (300 nM) used in the melting experiments observing fluorescence were different. The extent-of-melting curves derived from the UV absorption curve (see Figure 4D) were corrected for the concentration difference between the samples according to the extended all-or-none model (see Appendix); this correction shifts the T_m (see eq A-8).

Concentration Dependence of the T_m. The effect of the oligonucleotide concentration on the melting temperature of the 16-bp doubly labeled duplex was studied. Melting curves were taken at four different concentrations: $c_0 = 68$, 136, 408, and 1556 nM, where c_0 is the total concentration of each strand. Each melting curve was fitted independently according to the extended all-or-none model as described above, and the ΔH and ΔS of the duplex−random coil transition were determined. The ΔH_{hp} and ΔS_{hp} of the hairpin−random coil transitions were determined from experiments with the TMRh-labeled single strands (see above). The concentration of each reaction component (the duplexes, [ds], the hairpins, $[hp_1] = [hp_2] = [hp]$, and the random coil species $[rc_1] = [rc_2] = [rc]$) can be determined at any particular temperature from knowledge of the total strand concentration and the thermodynamic parameters of the helix−coil equilibria; thus the temperature where [ds] = [rc] can be found. We define the temperature where [ds] = [rc] as the melting temperature, T_m, of the ds → rc transition, and we define c as $c = [ds] + [rc]$. The determined molar enthalpy and entropy changes of the ds → rc and hp → rc reactions were used to calculate the values of T_m and c at $T = T_m$ at the different total concentrations used in the melting experiments (see eqs A-7 of the Appendix). According to the all-or-none model the dependence of T_m on c (see Appendix) is

$$T_m = \Delta H/(\Delta S - R \ln(c/2)) \quad (7A)$$

$$1/T_m = -(R/\Delta H) \ln c + (\Delta S + R \ln 2)/\Delta H \quad (7B)$$

It is important to note that c is different from c_0; $c_0 = c + [hp]$. The reciprocals of the T_m values versus ln c are plotted in Figure 6; this graph should be linear (see eq 7B) if the all-or-none model for the duplex−random coil transition pertains. The slope of this curve is equal to $R/\Delta H$, and the intercept on the $1/T_m$ axis is $[\Delta S + R \ln(2)]/\Delta H$. The average ΔH and ΔS values determined from the slopes and intercepts are shown in Table 2. The errors of the values of $1/T_m$ are on the order of the differences between the $1/T_m$ values determined from the different fluorescence parameters (see Figure 6).

DISCUSSION

Before discussing details of the results there are several general aspects that can be considered. The thermal denaturation experiments were carried out under equilibrium conditions; therefore, the underlying description of the results is based on statistical thermodynamics. The molecular thermodynamic description must be independent of the signal that has been selected for following the progress of the

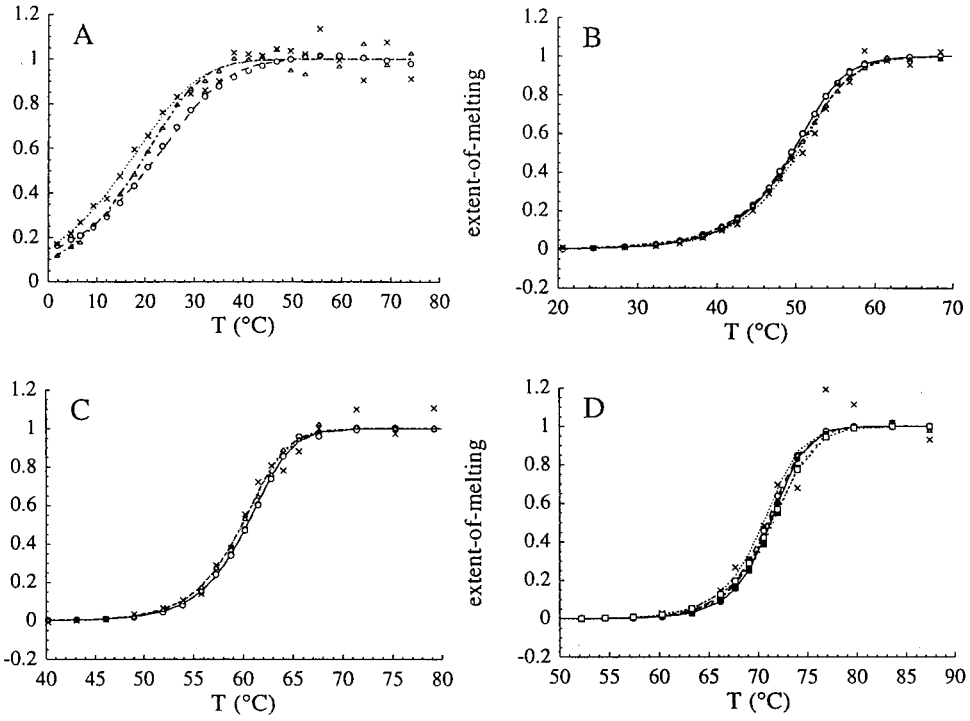

FIGURE 4: Temperature dependence of the extent-of-melting of the duplexes. The extent-of-melting versus temperature curves were derived from fits of the temperature dependence of the fluorescence intensity of fluorescein (△), fluorescence intensity (●) and anisotropy (○) of TMRh, $(\text{ratio})_A$ (×), and UV absorption heating (□) and cooling (■) curves. The fits (lines) correspond to an extended all-or-none model including duplex, hairpin, and random coil forms of the oligonucleotides. The actual value of the extent of melting means the sum of the hairpin and random coil fractions. (A) Eight-base pair duplex: the discrepancy between the curves derived from the different parameters is probably due to a fitting error caused by a baseline error in the double-stranded form. (B) Twelve-base pair, (C) sixteen-base pair, and (D) twenty-base pair duplexes. The good agreement between the extent-of-melting curves (T_m's are equal to within 1 degree K) suggests that fraying of the ends does not occur to an extent detectable by our multiparameter comparison.

denaturation reaction; however, the deconvolution of spectroscopic data in terms of a molecular model is never unique, and it is better to procure additional information by observing several different spectroscopic signals. The temperature denaturation curves corresponding to the different spectroscopic signals all have unique characteristic temperature profiles. The molecular processes occurring in the wings of the main transition of the melting curve are quite diverse: static and dynamic quenching, temperature-dependent molecular rearrangements of the TMRh between distinct TMRh−DNA isomeric configurations (see Figure 7), temperature-dependent formation of hairpins in certain single-stranded molecules, temperature-dependent variations in the absorption coefficients of the dye−DNA complexes, and changes in the rate of rotational diffusion resulting in changes in the fluorescence anisotropies of the dyes and nonlinearities in certain parameters, such as $(\text{ratio})_A$ and anisotropy. Many of these parameters affect the ultimate calculation of the extent-of-melting and the temperature dependence of the FRET efficiency. Information about the molecular processes in the wings of the main transition (the baselines) is crucial for making a reasonable interpretation of the data in the region of the major transition of the duplex−single-stranded denaturation reaction. The variety of spectroscopic effects in the baselines leads to the disparate appearance of the profiles of the different raw melting curves. However, as can be seen in Figure 4, when these molecular events are correctly taken into account in the baselines, the descriptions of the actual duplex−single-stranded transitions are very similar, regardless of which spectroscopic parameter is used to follow the melting transition, even for the case of the 8-bp duplex, where the apparent T_m values of the raw spectroscopic melting curves vary widely. This increases our confidence in our interpretation of the molecular processes participating in the baselines of the spectroscopic melting curves, as well as in the ultimate thermodynamic interpretation of the major duplex−single-stranded thermal transition.

The fluorescence parameters of TMRh and fluorescein attached to the 5′-end of DNA oligonucleotides are effective indicators of the helix−coil transition.

To allow a meaningful *quantitative* analysis of the helix−coil transition, a parameter chosen for following the melting transition must be measured accurately and it is better if its relative change upon melting is not too small. These conditions are fulfilled by the fluorescence intensity of both dyes, the fluorescence anisotropy of TMRh, and $(\text{ratio})_A$ (a parameter characterizing the efficiency of FRET). It is reasonable to assume that the fluorescence intensity is dependent on the double- or single-stranded character of the nucleotides mainly at the end of the molecule where the dye is located, whereas the anisotropy probably depends both on the state of the few nucleotides in the vicinity of the dye, and on the overall state of the molecule, and the efficiency of FRET depends on the distance and relative orientation between the reporter dyes at opposing ends of the duplexes.

The TMRh-Labeled Single Strands Can Form Hairpins. Many of the melting profiles can only be interpreted reasonably if the presence of the hairpins is taken into account, and this is especially true if the values of the thermodynamic parameters for the duplex−single strand transition are to be determined "correctly". We discuss first the formation of the hairpins of the single-stranded oligo-

Table 2: The Thermodynamic Parameters of the Duplexes[a]

duplex length	parameter	ΔH (kcal/mol)	ΔS (cal/mol/K)	ΔG (kcal/mol)	ΔH/bp (kcal/mol)	ΔS/bp (cal/mol/K)
8 bp	*F*(490,518)	58 ± 8	158 ± 21	10.9	7.2 ± 1.0	19.8 ± 2.7
	r(560,590)	65 ± 8	185 ± 23	9.8	8.2 ± 1.0	23.1 ± 2.9
	ratio A	61 ± 6	173 ± 21	9.4	7.7 ± 0.8	21.6 ± 2.6
	nearest n. estimate	56			7.0	22−24
12 bp	*F*(560,590)	97 ± 5	269 ± 17	16.8	8.1 ± 0.5	22.4 ± 1.4
	F(490,518)	93 ± 5	257 ± 17	16.4	7.8 ± 0.4	21.4 ± 1.4
	r(560,590)	88 ± 5	242 ± 15	15.8	7.4 ± 0.4	20.2 ± 1.3
	ratio A	94 ± 9	260 ± 30	16.5	7.9 ± 0.8	21.7 ± 2.5
	nearest n. estimate	92			7.7	22−24
16 bp	*F*(560,590)	134 ± 10	380 ± 29	20.7	8.4 ± 0.6	23.8 ± 2
	F(490,518)	136 ± 8	378 ± 25	23.3	8.5 ± 0.5	23.6 ± 1.6
	r(560,590)	137 ± 12	389 ± 31	21.0	8.6 ± 0.7	24.3 ± 2.2
	ratio A	139 ± 9	389 ± 30	23.0	8.7 ± 0.6	24.3 ± 1.9
	UV abs	122 ± 28	333 ± 85	22.7	7.6 ± 1.8	20.8 ± 5.3
	from $1/T_m$ vs ln(*c*)	153 ± 18	425 ± 53	26.3	9.5 ± 1.1	26.6 ± 3.3
	nearest n. estimate	118			7.4	22−24
20 bp	*F*(560,590)	182 ± 8	497 ± 23	33.8	9.1 ± 0.4	24.9 ± 1.2
	F(490,518)	175 ± 5	478 ± 16	32.5	8.7 ± 0.3	23.9 ± 0.8
	r(560,590)	170 ± 8	464 ± 22	31.7	8.5 ± 0.4	23.2 ± 1.1
	ratio A	170 ± 8	468 ± 22	30.5	8.5 ± 0.2	23.4 ± 0.6
	UV abs	162 ± 13	439 ± 39	31.1	8.1 ± 0.7	22 ± 2
	nearest n. estimate	154			7.7	22−24
34 bp	*F*(560,590)	194 ± 20	533 ± 55	35.1	5.7 ± 0.6	15.7 ± 1.6
	nearest n. estimate	252			7.4	22−24

[a] The molar enthalpy (ΔH) and entropy (ΔS) changes of the helix−random coil transition of the 8-, 12-, 16-, and 20-bp doubly labeled duplexes were determined by nonlinear fits of the different spectroscopic parameters according to the extended all-or-none model; this model assumes the presence of three conformations: the fully base-paired duplex, the fully base-paired hairpin, and the random coil. The ΔH and ΔS for the 34-bp duplex was determined according to the all-or-none model assuming only duplex and random coil conformations (no hairpins). The tabulated values of ΔH and ΔS are averages of n measurements ($n = 5$ for the 16-bp, $n = 2$ for the 20-bp, and $n = 1$ for the 8-, 12-, and 34-bp duplexes). The errors are either standard deviations of several measurements or error estimates yielded by the nonlinear fits of the melting curves. The values of ΔG ($T = 25$ °C) are also given.

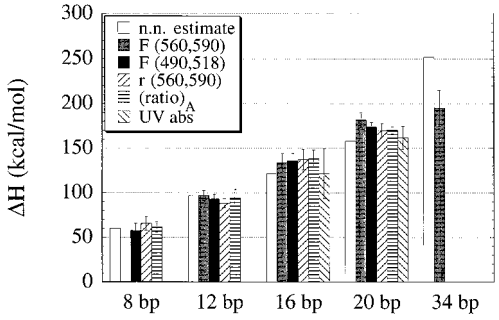

FIGURE 5: Standard enthalpy change accompanying the dissociation of the duplexes. The ΔH values correspond to the molar enthalpy difference between the random coil and duplex forms determined according to an extended all-or-none model dealing with duplexes plus hairpin and random coil states of single strands. ΔH values were extracted from the melting curves of the fluorescence intensity (exc, 560; em, 590; gray bars) and anisotropy (ex, 560; em, 590; ⧄) of TMRh, the intensity of fluorescein (exc, 490; em, 518; ■), $(\text{ratio})_A$ (bars with horizontal stripes), and UV absorption (⧅) by nonlinear least-squares fitting technique. The plotted ΔH values are averages of n measurements; for the 16-bp duplex ($n = 5$) and the 20-bp duplex ($n = 2$) the error bars are standard deviations of the values obtained in the individual measurements. For the 8- and 12-bp duplexes $n = 1$; error bars indicate the estimated error of ΔH from the fit of the melting curves. The predicted values of ΔH (□) calculated by summing the nearest-neighbor enthalpies of hydrogen-bonding and base-stacking interactions are shown for comparison (*15*).

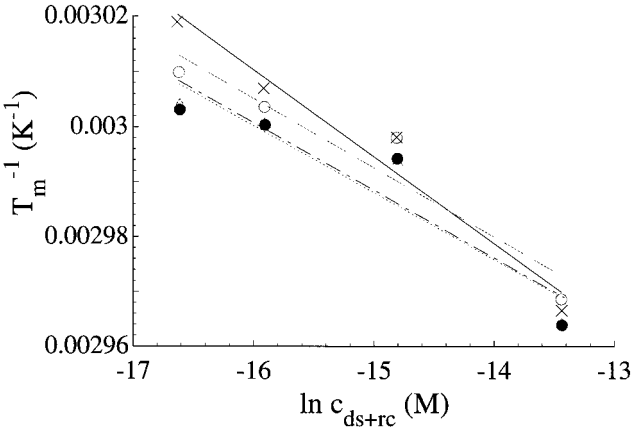

FIGURE 6: Dependence of the melting temperature of the 16-bp duplex on the concentration of the sample. T_m values of the duplex−random coil transitions, where the duplex and random coil conformations have equal concentrations, that is, $[ds] = [rc_1] = [rc_2]$ were determined (see text) from the melting curves of the fluorescence intensity (●) and anisotropy (○) of TMRh, the fluorescence intensity of fluorescein (△), and $(\text{ratio})_A$ (×). The $1/T_m$ versus ln(*c*) function should be linear according to the two-state model of melting, while the statistical mechanical description based on the evaluation of the partition function of the molecule should yield a concave-up curve; our curves are concave-down. The average ΔH and ΔS of the helix−coil transition calculated from the slopes and intercepts of the straight-line fits are shown in Table 2.

nucleotides because this reaction must be included in the final analysis of the duplex−single strand transition. Our results show that the TMRh-labeled single strands with GG-3′ at the 3′-end can form hairpins. Figure 8 shows possible Watson−Crick base pairs consistent with the sequences. Our presumption of hairpin formation is based on the comparison of the temperature profiles of the fluorescence parameters of the duplexes (see Figure 2) and the single strands (see Figure 1). Four strong arguments for hairpin formation are the following: (1) For those single-stranded oligonucleotides

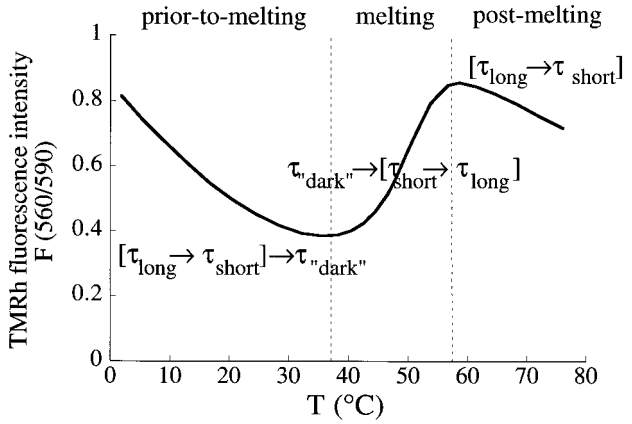

FIGURE 7: The temperature-dependent redistribution between the different TMRh−DNA complexes. The change of the temperature affects the equilibria between the three different lifetime states of the TMRh−DNA complex: a short lifetime state ($\tau \sim 1$ ns), a long lifetime state ($\tau \sim 3-4$ ns), and a "dark" (low quantum yield) state (*17*). The changes of the fluorescence intensity and anisotropy are understandable in light of the transitions between the three species in the different regions of the melting curve. The transitions in brackets are observable directly by measuring the time-resolved parameters of fluorescence; the transitions involving the dark state can be deduced by indirect methods, for example by comparing the temperature dependence of the mean lifetime and the steady-state intensity (*17*).

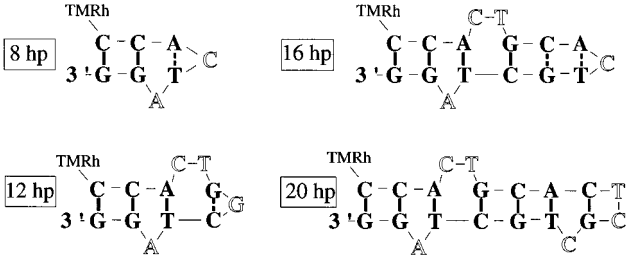

FIGURE 8: Possible structure of the hairpin molecules. The possible Watson−Crick base pairs are shown. The vertical solid lines between the bases represent the number of base pairs that are probably formed as indicated by the ΔH and ΔS of the melting transition; the vertical dashed lines between the bases indicate hydrogen bonds that could also be formed. The standard enthalpy changes accompanying the melting of the 8-, 12-, 16-, and 20-base hairpin molecules are shown in Table 1.

that could form hairpins, the fluorescence intensity of the attached TMRh molecules increases as the temperature is raised (see Figure 1A) similarly to a thermal denaturation curve of the duplex (see Figure 2A). In the duplex, this increase has been attributed to the helix−coil transition of the bases at the 5′-end of the molecules where the dye is attached (see below). (2) The TMRh anisotropy decreases abruptly as the temperature is raised in the same temperature range where the fluorescence intensity increases; this is consistent with the increased mobility of the dye when its environment changes from a duplex state to a random coil state. (3) The "T_m" of the melting of the hairpins was not affected by using two concentrations differing by a factor of 10 (data not shown), which is to be expected for a monomolecular transition. (4) Our proposal of hairpin formation with the single-stranded oligomers was corroborated by the melting experiments using the 8- and 16-bp strands with CC rather than GG at the 3′-ends. As expected, this change prevented base pair formation between the 5′- and 3′-ends of the molecule. The temperature profiles

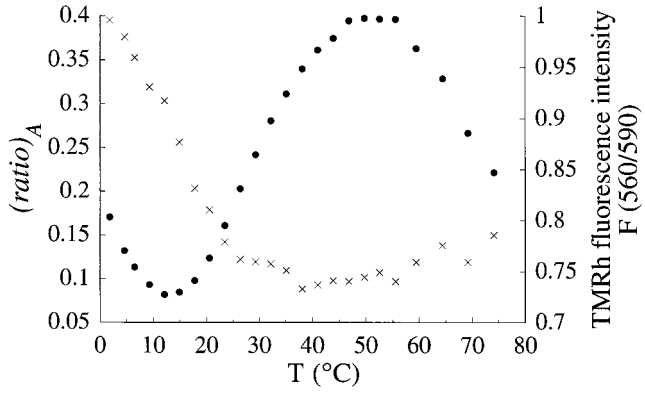

FIGURE 9: The melting curves of the 8-bp duplex, monitored by $(\text{ratio})_A$ (×) and the fluorescence intensity of TMRh (●). The continuously decreasing tendency of $(\text{ratio})_A$, which is linearly dependent on the efficiency of FRET, implies that strand dissociation is under way at the very beginning of the melting curve. On the other hand, the fluorescence intensity of TMRh, which is supposed to increase upon the opening of the end of the duplex, shows that the 5′-end where the TMRh dye is situated is still in a base-paired state. This is direct evidence of hairpin formation of the dissociated TMRh-labeled strand.

of the 8-base and the 16-base single-stranded CC-3′ oligomers are shown in Figure 1. The decrease of the fluorescence intensity and anisotropy curves of the 8- and 16-base single strands is smooth, lacking any abrupt variation attributable to the denaturation of hairpins.

We analyzed the fluorescence intensity melting curves of the hairpins assuming that the melting of the hairpin structure takes place in an all-or-none manner (for the thermodynamic equation describing the process, see the Appendix). If we assume that the enthalpy change is about 8 kcal/mol per base pair, the van't Hoff enthalpies and entropies in Table 1 imply that, especially for the 16-base strands, fewer base pairs are formed than shown in Figure 8. Another equally possible explanation for the value of the total two-state enthalpy is that the stability of some of the base pairs in the hairpins is lower than in a normal duplex, even though all base pairs shown in Figure 8 are formed. We cannot distinguish these two possibilities. The melting process of the hairpins involves only a small number of base pairs, and therefore, the transitions are broad and the baselines must be determined over a large temperature range. The uncertainty in fitting the curved baselines leads to more uncertainty in the ΔH values of the hairpins than for the duplexes (Table 1). However, including the thermodynamic and spectroscopic influence of the hairpins greatly improved the analysis of the melting of the duplexes, especially in the case of the 8-bp duplex (Figures 4 and 9).

The hairpin formation can be easily observed because the fluorescence intensity and anisotropy are sensitive to the local environment of the dyes. Fluorescence is an excellent parameter for following the formation of hairpins. This would be difficult to do with other methods such as absorption in the nanomolar concentration range because of the low number of base pairs involved; absorption would require micromolar concentrations. The existence of hairpins stabilized by 2 base pairs has been shown using NMR (*36*), but this technique requires even higher concentrations, on the order of a few millimolar.

The Baselines of the Melting Curves. To analyze the melting curves properly, a detailed knowledge of the

baselines is required. Unquestionably, the best way to determine the baselines is to measure individually the spectroscopic parameters of the ds and ss species. It is possible to determine the temperature dependence of the spectroscopic parameters of the single-stranded species using the single strands of the duplexes. The double-strand baselines are more difficult to determine. By increasing the concentration of the sample, which shifts the T_m to a higher temperature, the more extended double-strand region of the melting curve can be used as a baseline for a sample having a lower concentration and a lower T_m. Unfortunately, this possibility is often limited by the amount of sample. In such cases it is helpful to have a physically reasonable model for the spectroscopic behavior of the ds species to extrapolate the double-strand baseline in the melting region where no experimental data for the pure species are available.

For the absorption melting curves and the fluorescence melting curves following the intensity of fluorescein, the nonlinearities of the baselines are probably negligible, and therefore, no single-stranded samples for the absorption baselines were measured. For these data the baselines were fitted well with straight lines.

On the other hand, the fluorescence intensity of TMRh in the ds form of the duplex deviated significantly from a straight line. This is due to a temperature-dependent rearrangement among the multiple conformations of the TMRh−DNA complex that are present (*17*): two fluorescent species with lifetimes of ∼3−4 and ∼1 ns and a third nonfluorescent (low quantum yield), "dark" species. The equilibrium among these states shifts toward the dark state and toward the shorter-lifetime state as the temperature is increased, resulting in a decrease of the fluorescence intensity (see Figure 7). In the baseline region of the pure duplex, the temperature dependence of the duplex fluorescence intensity, F_{ds}, could be fitted well according to a simple model of a monomolecular transition between two fluorescent states with differing molar fluorescence intensities. Inclusion of a further state, for example, the dark state, in the calculations did not improve the fit but simply increased the redundancy and uncertainty of the parameters. Using this model it was possible to fit the lower baselines of all the TMRh melting curves.

The $(\text{ratio})_{A,ds}$ and $(\text{ratio})_{A,ss}$ baselines were approximated by straight lines. Both baselines of $(\text{ratio})_A$ increase with increasing temperature. The increasing $(\text{ratio})_{A,ss}$ baseline can be accounted for completely by the shifts and the changes in shapes of the different spectral regions of the absorption spectrum of TMRh. The efficiency of energy transfer is 0 in the single-stranded state, so the value of the single-stranded baseline is (see eq 4) the following:

$$(\text{ratio})_{A,ss} = F^A(490,590)/F^A(560,590) = \epsilon^A(490)/\epsilon^A(590) \quad (8A)$$

With increasing temperature the value of $\epsilon^A(490)$ increases and $\epsilon^A(590)$ decreases, and their ratio varies with temperature as does the experimental $(\text{ratio})_{A,ss}$ data (see Figure 2D).

The double-strand baseline of $(\text{ratio})_{A,ds}$ is (where energy transfer is present)

$$(\text{ratio})_{A,ds} = \frac{\epsilon^D(490)}{\epsilon^A(560)}E + \frac{\epsilon^A(490)}{\epsilon^A(560)} \quad (8B)$$

The ratio $\epsilon^D(490)/\epsilon^A(590)$ is also an increasing function of the temperature; however, the increase of the $(\text{ratio})_{A,ds}$ baseline can only partially be explained by the temperature dependence of the ratio of absorption coefficients (*37*). The remainder of this increase is apparently due to an increase in FRET resulting from an increase in the overlap integral and from the temperature-dependent redistribution of the TMRh molecule on the duplex DNA structure. As the temperature is increased, the peak of the emission spectrum of the fluorescein label (donor) is shifted to the red (521.5 → 523.5 nm between 0 and 80 °C), and the absorption peak of the TMRh label (acceptor) is shifted to the blue (560 → 556 nm between 0 and 80 °C). This slightly increases the overlap between the two spectra and thereby increases the FRET efficiency contributing to the increase of the $(\text{ratio})_{A,ds}$ baseline. The contribution of the TMRh redistribution to the increasing baseline is discussed in the following section.

The ds baseline r_{ds} of the TMRh anisotropy was fitted to a straight line, whereas the single-stranded baseline r_{ss} was determined experimentally with the TMRh-labeled strand. The temperature dependence of the equilibrium between the two fluorescent conformations of the TMRh−DNA complex contributes to the temperature response of the anisotropy, in addition to the usual change of the rotational diffusion of the probe. Fortunately, the shapes of the double-strand baselines of the anisotropy are very close to straight lines for the 12- and 16-bp duplexes. The temperature dependence of the anisotropy of the 20-bp duplex in the double-stranded form is nonlinear (see Figure 2C); this phenomenon will be discussed in the next section.

The Effect of the Existence of Multiple TMRh−DNA Complexes on the Spectroscopic Parameters of the Dyes and on the Efficiency of FRET below the T_m. The temperature-dependent redistribution among the different conformations of the TMRh−DNA complex influences several of the measured spectroscopic parameters; these effects are quite apparent in the melting profile of the 20-bp duplex. We (*17*) have shown that the equilibrium between the 4- and 1-ns lifetime states is shifted toward the shorter lifetime state as the temperature is raised, which causes the average lifetime of the TMRh to decrease. The majority of this isomerization of the TMRh−DNA complex takes place between 20 and 40 °C. The shift to the shorter lifetime component is accompanied by an increase in the anisotropy (see Figure 2C) and a decrease of the fluorescence intensity (see Figure 2A) of the TMRh label on the 20-bp duplex molecules. In the same temperature range the fluorescence parameters of the fluorescein label and the $(\text{ratio})_A$ curve are also affected by this change in the TMRh configuration. The fluorescence intensity of the fluorescein drops (see Figure 2B), and its anisotropy (see Figure 2E) shows a slower decrease with increasing temperature than either below or above this range; $(\text{ratio})_A$ (see Figure 2D) increases rapidly in this temperature range. All of these effects imply that the efficiency of FRET increases, decreasing the fluorescence lifetime of the fluorescein. Perhaps the relative orientation of the TMRh and fluorescein dipoles is more favorable or the distance between the two dyes is shorter, when the TMRh−DNA complex is

in the 1 ns lifetime state. The last four bases of the sequence of the 8-, 12-, 16-, and 20-bp molecules are identical in all the duplexes. However, the influence of the transition between the different lifetime states on the spectroscopic parameters is most prevalent in the melting curves of the 20-bp molecule.

Temperature Profiles of the Fluorescence Intensity of TMRh and Fluorescein through the ds−ss Transition Region. We have shown (*17*) that a larger molecular fraction of the TMRh−DNA complex is in the dark state in the duplex form than in the single-stranded form at any particular temperature. In addition, the fluorescence lifetimes are slightly longer, and the molecular fraction of the long lifetime state is also larger in the single-stranded state than in the duplex state. As a consequence, the apparent overall quantum yield of TMRh is greater in the single-stranded form than in the double-stranded form, and the melting is accompanied by an increase of the fluorescence intensity (see Figure 2A). The inherent fluorescence intensity of fluorescein (e.g., duplexes labeled with only fluorescein; data not shown), which is located at the opposing 5′-end of the duplex with respect to the TMRh label, also increases upon melting (see Figure 2B). However, the fluorescein fluorescence intensity is also diminished by energy transfer in molecules doubly labeled with fluorescein and TMRh. If the fluorescence intensities of the different duplexes are normalized in the ss-region, the longest molecule, the 20-bp duplex, has the highest fluorescence intensity in the duplex state because the energy transfer for this molecule is the lowest, Figure 2B.

Temperature Profiles of the Fluorescence Anisotropy of TMRh and Fluorescein through the ds−ss Transition Region. The abrupt decrease of the anisotropy as the temperature is increased to the range where strand dissociation takes place (see Figure 2C) suggests that the mobility of the TMRh label is greater in the single-stranded form than in the double-stranded form. In addition, the equilibrium between the short and long lifetime states of the TMRh−DNA complex is shifted toward the state with a longer lifetime as the strands dissociate; this also contributes to the decrease of the anisotropy. This has been found in all of our previous measurements (*1*, *17*). The anisotropy of the fluorescein label is much lower than that of the TMRh label at all temperatures, indicating that the interaction between the oligomer and the fluorescein label is looser and the mobility of the dye is higher than for TMRh. The anisotropy of fluorescein is already low in the double-stranded form, and the change of the anisotropy upon melting is small; this makes it difficult to analyze the melting transition quantitatively by using the fluorescein anisotropy data. Because of FRET, which lowers the lifetime of the donor (thereby increasing its anisotropy), the fluorescence anisotropy of duplex molecules singly labeled with fluorescein (data not shown) is lower than that of doubly labeled molecules. The value of the anisotropy of the fluorescein is the lowest for the 20-bp duplex because this molecule has the least energy transfer so that the fluorescence lifetime is the longest (see Figure 2E).

FRET Melting Curves. Changes in the efficiency of FRET from the $(\text{ratio})_A$ values can be calculated at every temperature (see eq 4). However, in a mixture of different species (see eq 6), for example, duplexes and single strands, the value of $(\text{ratio})_A$ does not depend linearly on the molar fractions because terms proportional to the molar fractions are present in the denominator as well as in the numerator in the expression for $(\text{ratio})_A$ (see Appendix for derivation). Therefore the $(\text{ratio})_A$ melting curves cannot be analyzed simply as the fluorescence intensity melting curves. In the event that the $(\text{ratio})_A$ melting curves are analyzed according to an equation similar to eq 5, the calculated extent-of-melting curves are displaced to a lower temperature; this displacement is an artifact, resulting simply from the terms proportional to the molar fractions of the duplex and single-stranded states of the oligonucleotides in the denominator. If a correct analysis is made of the $(\text{ratio})_A$ curves, as shown in the Appendix, then the calculated extent-of-melting curve is not offset, as shown in Figure 4, and the FRET extent-of-melting curve agrees with the extent-of-melting curves calculated directly from the fluorescence intensities.

With the knowledge of the temperature dependence of the appropriate absorption coefficient ratios (see eq 4), the efficiency of FRET, E, could be determined. However, the knowledge of E is not required in order to determine the extent-of-melting from the FRET data; the temperature dependence of $(\text{ratio})_A$ can be evaluated directly. The advantage of $(\text{ratio})_A$ is that it is a more directly determined parameter than E. It does not necessitate the measurement of the temperature dependence of the absorption coefficients; therefore its measurement is easier and its error is smaller. As long as the baselines of $(\text{ratio})_A$ are approximately straight, the determination of the absorption coefficient ratios can be avoided. Imperfect labeling of the oligonucleotides would change the value of $(\text{ratio})_A$, but it would not influence the temperature profile of the extent-of-melting curves determined from the $(\text{ratio})_A$ versus temperature curves.

Temperature Profiles of the Mean Lifetime of TMRh. Assuming that the fluorescence lifetime of a species is proportional to its quantum yield and all the species are taken into account with their corresponding molar fractions when calculating the mean lifetime (according to eq 1), the shapes of the mean lifetime and the steady-state fluorescence intensity curves should be identical.

However, the percent decrease of the steady-state intensity is greater than that of the mean lifetime in the same temperature range of 5−60 °C. Both parameters follow a similar decreasing tendency in the double-stranded range and an increasing tendency in the temperature range where the melting takes place. The decrease of the mean lifetime and steady-state intensity in the duplex state as the temperature increases is due to the shift of the equilibrium between the two fluorescing states toward the shorter lifetime state (*17*). The steady-state fluorescence intensity is further diminished by the increase of a population in a dark state (low quantum yield), but the presence of this dark state does not affect the observed lifetimes. This causes a discrepancy between the measured steady-state intensity and the mean lifetime and indicates that the dark state becomes more populated in the duplex state as the temperature is increased.

The mean lifetime (eq 1) is greater in the single- than in the double-stranded form. In the single-stranded state the lifetimes are slightly longer and the molecular fraction of the longer lifetime component is greater than in the duplex state. It has been shown by Vámosi et al. (*17*) that the dark state is probably less populated in the single-stranded form

than in the double-stranded form.

The Analysis of the Melting Curves of the 12-, 16-, and 20-bp Duplexes According to the Extended All-or-None Model Yields Good Agreement between Data Sets Taken with Different Spectroscopic Parameters. The extended all-or-none model (see Appendix) fits the melting curves of the 12-, 16-, and 20-bp duplexes well. The extent-of-melting curves (see Figure 4) and the thermodynamic parameters (see Figure 5 and Table 2) are nearly identical when derived from the different fluorescence parameters and from the UV absorption melting curves (for the 20-bp duplex). During the melting of these duplexes the presence of partially melted intermediates other than the hairpins is not detectable. This does not exclude a more complex mechanism of melting, such as a zipper model, but shows that a more complex model is not required.

Morrison and Stols (*12*) observed by FRET that the equilibrium properties of the melting reaction mixture of 10- and 20-bp duplexes could be described adequately with an all-or-none model. Their sequences could not form stable hairpins; however, their kinetic data suggest that the *mechanism* of the helix−coil transition is more complex than the two-state model. By observing the temperature-induced spectral shift of a modified fluorescent base, 2-aminopurine, Xu et al. (*13*) have shown that a premelting transition purely dynamic in nature can be observed prior to melting of the B-helical structure.

Concentration Dependence of the T_m of the 16-bp Duplexes. The determination of ΔH and ΔS from the concentration dependence of the T_m is thought to be a fairly robust analysis (*38*). In our calculations we defined T_m as the temperature where the molecular fractions of the strands that are in duplex and random coil conformations are equal; this is not $^1/_2$ of the total number of strands because the hairpins are also present. This T_m is different from the "apparent" melting temperature where half of the molecules have dissociated and are either in the hairpin or in the random coil form. The graph of $1/T_m$ versus ln$c$, where c is the sum of the concentrations of the duplex and random coil forms, should be linear according to the all-or-none model. Though the actual graphs in Figure 6 are not linear, the ΔH and ΔS values determined from the slopes and intercepts compare well with the values derived from the nonlinear fits of the individual melting curves and with the nearest-neighbor estimates. We cannot definitely account for the downward concave shape of the $1/T_m$ versus ln$c$ curves, but some possibilities can be ruled out. When analyzing the melting curves according to the two-state model without taking into account the presence of the hairpins, the shapes of the $1/T_m$ versus ln$c$ curves are very similar to those shown in Figure 6 (data not shown). Simulations according to the statistical zipper model have shown that the presence of partially melted intermediates would yield an upward concave curve; thus the shape of the curves cannot be explained by the presence of further intermediate states, either. The shape might be due to experimental error in the measurement of the temperature in the individual melting curves or to inaccuracy in the determination of the energetic parameters of the melting of the hairpins. Finally, we cannot exclude the possibility that the melting process, or the coupling of the spectroscopic signals to the molecular process of melting, is more complicated than assumed in our models.

Comparison of the Melting Curves of the 8-bp Duplex Taken with Different Spectroscopic Parameters. The effect that the different spectroscopic parameters have on the observed melting curves can be seen most effectively by comparing the melting curves of the different fluorescence parameters of the 8-bp duplex. It was the melting behavior of this duplex when followed by measuring the fluorescence intensities and $(\text{ratio})_A$ that made us realize that the melting process of the duplexes is not a simple bimolecular equilibrium of the random coil and duplex conformations. For the sake of comparison, the melting curves of the fluorescence intensity of TMRh and $(\text{ratio})_A$ were plotted together in Figure 9. The decrease of $(\text{ratio})_A$ suggests that melting is under way at the lowest temperature of the measurement. The fraction of dissociated strands at 1.8 °C is about 10% according to our analysis. On the other hand, the fluorescence intensity continues to decrease with increasing temperature between 0 and 12 °C, where there are major changes in the $(\text{ratio})_A$ values. The expected increase of the fluorescence intensity as the end of the DNA molecule, where TMRh is attached, becomes single-stranded is apparent only above 12 °C. $(\text{ratio})_A$ and the fluorescence intensity of TMRh display substantially different apparent T_m values; $(\text{ratio})_A$ shows earlier melting. In a paradoxical way strand dissociation seems to precede the opening of the end of the molecule. This discrepancy can be resolved by assuming that the dissociated TMRh-labeled strand can fold back on itself forming a hairpin with a locally base-paired structure at the end of the molecule, delaying the increase of the fluorescence intensity of the TMRh fluorescence curve.

Melting Curves of the 34-bp Duplex. The 34-bp duplex molecule is considerably longer than the other duplexes studied in the present paper. Thus the melting process of this duplex can be expected to deviate most from the two-state mechanism. Even though the TMRh-labeled single strands can form a hairpin, the hairpin is not stable in the temperature range of the main duplex−single strand transition; therefore, the inclusion of this species in the thermodynamic analysis is not necessary. However, the fluorescence intensity melting curve of this molecule is not fitted well by the all-or-none model (Figure 3A). In addition, the ΔH determined from the two-state fit is only ~77% of the value estimated by adding the nearest-neighbor interaction terms available in the literature (*15*) (see Table 2). This discrepancy, which is not apparent for the shorter oligonucleotides, is indicative of the presence of intermediates; the presence of more intermediate states causes the broadening of the transition and this leads to decreased apparent values of the expected energetic parameters if the transition is analyzed as two-state.

The extent-of-melting, α, was simulated according to a statistical mechanical zipper model of the melting (see Figure 3B); in this model the base pairs can open up (become unbase-paired) from both ends, but no internal loops are allowed; internal loops are highly improbable because of their relatively low entropy contribution (*16*). In our simulation we assumed that presence of the helix or coil state of only a certain number of base pairs at certain positions of the duplex affects the fluorescence signal. The varied parameters during the simulation were the average $\langle \Delta H_{bp} \rangle$ belonging to the opening of a base pair, and the position of the base pairs influencing the signal from one selected molecule. It was

found that the data are best represented by the simulation if we assume that only the last 5 base pairs have an effect on the signal originating from a given molecule. Of course, the state of the other bases also influences the *total* fluorescence signal from the sample through the statistical weights by which the different intermediate conformations are represented in the partition function of the molecule.

The shape of the simulated curve is a very sensitive function of the parameters of the simulation, such as the ΔH and ΔS of the formation of a given base pair at a certain position of the duplex. This sensitivity is the strength and weakness of simulations with such a multivariable model, but the statistical model represents the actual molecular situation better than the two-state model. It is therefore necessary to pick reasonable average values for the parameters and to introduce variations only if the molecule has special features such as mismatched or bulged nucleotides or junctions (see, for example, refs *37* and *39*; Gohlke et al., in preparation). In our case of a simple 34-bp duplex, it was sufficient to use average ΔH and ΔS values to represent the melting curve with reasonable accuracy, but the two-state model is insufficient.

CONCLUSIONS

Because fluorophores are sensitive indicators of their physical-chemical surroundings, the spectroscopic parameters of fluorophores attached covalently to oligonucleotides are useful tools for studying the helix−coil transition of these macromolecules. The different fluorescence parameters, the fluorescence intensity and anisotropy of TMRh, the intensity of fluorescein, and the efficiency of energy transfer between fluorescein and rhodamine, all provide disparate views of the melting process; in some cases the information provided by the different parameters is complementary. These fluorescence parameters can be measured with sufficient accuracy and their change upon melting is large enough so that they can be used for the quantitative analysis of the helix−coil transition.

The shapes of the baselines of the fluorescence parameters related to TMRh can be understood in terms of the temperature-dependent equilibrium between several conformations of the TMRh−DNA complex. The knowledge of the baselines is crucial for the evaluation of the temperature profiles of the spectroscopic parameters. It is best to determine the baselines experimentally, for example, using single-stranded molecules; however if the experimental determination is not possible, the knowledge of the thermodynamic and photophysical properties of the different dye−DNA complexes is useful.

We observed that the single-stranded molecules with 5′-CC and GG-3′ ends can form hairpins stabilized by only a few base pairs. This is easily observable and identifiable in the fluorescence experiments. Changing the sequence to CC-3′ prevents hairpin formation completely in all oligonucleotides. The existence of hairpin structures must be taken into account in the statistical thermodynamic description of the dissociation of the duplexes made up of single strands that can form hairpins.

The helix−coil transition of the 8-, 12-, 16-, and 20-bp duplexes can be described well by the extended all-or-none model including only the fully base-paired duplex, the maximally base-paired hairpin, and the random coil conformations. The reaction mixture does not contain other partially melted intermediates in amounts perceptual by our methods. The thermodynamic parameters of the duplex−random coil transition determined from the temperature profiles of the fluorescence parameters compare well with the values derived from UV absorption melting curves and predictions based on the nearest-neighbor interaction values available in the literature. The extent-of-melting curves derived from the different spectroscopic observables show a good agreement.

The denaturation of the 34-bp duplex cannot be described sufficiently by the all-or-none model; the melting profile could be better simulated by the statistical zipper model. The shape of the apparent extent-of-melting curve changes sensitively depending on the region of the molecule that influences the signal. Assuming that the helix or coil state of the last 5 base pairs in the vicinity of the dye affects the signal gave the best agreement between the measured and simulated extent-of-melting curves. Fits assuming that bps 1−5, 2−5, or 3−5 affect the fuorescent signal gave similarly good agreement with the experimental data.

The simultaneous measurement of several parameters is necessary to resolve more complex molecular transitions. This was the case for the 8-bp duplex; strand dissociation was indicated by the decrease of FRET, while the opening of the 5′-ends of the duplexes or the single strands adopting hairpin conformation was shown by the change in the fluorescence intensity of TMRh. These overlapping processes could not have been resolved by following only one spectroscopic parameter. The measurement of the fluorescence parameters allows the investigation of the mechanism, thermodynamics and kinetics of the helix−coil transition, and other transitions of more complex macromolecules if they can be fluorescently labeled. These fluorescence parameters are sensitive to different aspects of the helix−coil transition and provide complementary information.

ACKNOWLEDGMENT

We thank D. M. J. Lilley, A. I. H. Murchie, C. Gohlke and F. Stühmeier for many discussions and collaborations on related topics, J. Szöllôsi for helpful criticism of the manuscript, A. Zechel for reading the manuscript, and S. Damjanovich for suggesting the collaboration between the authors.

APPENDIX

Calculating the Value of the Parameter (ratio)$_A$ for a Mixture. Just like fluorescence anisotropy, (ratio)$_A$ (see eq 4) is a ratio of fluorescence intensities. This is why the measured value of (ratio)$_A$ from a mixture of several species can be calculated from the characteristic (ratio)$_A$ values and the molar fractions of the different species in a manner similar to that of the calculation of the anisotropy of a mixture. Equations 2 and 4 in the text give the definitions of the anisotropy and (ratio)$_A$. The (ratio)$_A$ value of a mixture of duplex and single-stranded molecules is the following:

$$(\text{ratio})_A = \frac{F^{A(D)}(490,\lambda)}{F^{A(D)}(560,\lambda)} = \frac{(1-\alpha)F_{ds}^{A(D)}(490,\lambda) + \alpha F_{ss}^{A(D)}(490,\lambda)}{(1-\alpha)F_{ds}^{A(D)}(560,\lambda) + \alpha F_{ss}^{A(D)}(560,\lambda)} =$$

$$\frac{(1-\alpha)\dfrac{F_{ds}^{A(D)}(490,\lambda)}{F_{ds}^{A(D)}(560,\lambda)}F_{ds}^{A(D)}(560,\lambda) + \alpha\dfrac{F_{ss}^{A(D)}(490,\lambda)}{F_{ss}^{A(D)}(560,\lambda)}F_{ss}^{A(D)}(560,\lambda)}{(1-\alpha)F_{ds}^{A(D)}(560,\lambda) + \alpha F_{ss}^{A(D)}(560,\lambda)}$$

$$= \frac{(1-\alpha)(\text{ratio})_{A,ds}F_{ds}^{A(D)}(560,\lambda) + \alpha(\text{ratio})_{A,ss}F_{ss}^{A(D)}(560,\lambda)}{(1-\alpha)F_{ds}^{A(D)}(560,\lambda) + \alpha F_{ss}^{A(D)}(560,\lambda)} \quad \text{(A-1)}$$

where $(1-\alpha)$ is the fraction of duplexes in the mixture; α is the fraction of dissociated strands; $F_{ds}^{A(D)}(\lambda_1,\lambda_2)$ and $F_{ss}^{A(D)}(\lambda_1,\lambda_2)$ are the fluorescence intensities of the acceptor on the pure ds and ss species in the presence of the donor; λ_1 is the excitation and λ_2 is the emission wavelength; and $(\text{ratio})_{A,ds}$ and $(\text{ratio})_{A,ss}$ are the $(\text{ratio})_A$ values of the pure ds and ss species. Note that $(\text{ratio})_A$ in the single-stranded form is lower than in the double-stranded form because in the expression for $(\text{ratio})_A$ (see eq 4) $E = 0$ for single strands, that is, there is no energy transfer in the case of single strands.

The above expression can be generalized to any number of conformations by extending the sum to all conformations

$$(\text{ratio})_A = \frac{\sum_i \alpha_i(\text{ratio})_{A,i}F_i^{A(D)}(560,\lambda)}{\sum_i \alpha_i F_i^{A(D)}(560,\lambda)} \quad \text{(A-2)}$$

where α_i is the molecular fraction, $(\text{ratio})_{A,i}$ is the characteristic value of $(\text{ratio})_A$, and $F_i^{A(D)}(560,\lambda)$ is the molar fluorescence of the ith species.

Thermodynamic Models Describing the Helix−Coil Transition. (A) The All-or-None Model for the Dissociation of Duplexes. The dissociation of a duplex to two random coil molecules rc_1 and rc_2 is described by the van't Hoff equation for a bimolecular process:

$$K_d(T) = \frac{[rc_1][rc_2]}{[ds]} = \frac{c\alpha^2}{1-\alpha} = \exp\left(-\frac{\Delta H}{RT} + \frac{\Delta S}{R}\right),$$

$$A(T) = \frac{K_d(T)}{c} = \frac{\alpha^2}{1-\alpha},$$

$$\alpha(T) = \frac{-A(T) + \sqrt{A(T)^2 + 4A(T)}}{2} \quad \text{(A-3)}$$

where K_d is the dissociation constant, [ds], $[rc_1]$, and $[rc_2]$ are the concentrations of the duplex and coil molecules, $c = [ds] + [rc_1] = [ds] + [rc_2]$ (c is the total concentration of each strand), α is the molar fraction of coil molecules (or the extent-of-melting), ΔH and ΔS are the molar enthalpy and entropy change of the transition, R is the gas constant, and T is the temperature in K.

(B) The All-or-None Model for Monomolecular Transitions. The transition A → B between two states with different molar Gibbs free energies, such as the hairpin and random coil states of a DNA strand or two different TMRh−DNA complexes, is described by the van't Hoff equation for a monomolecular process:

$$K(T) = \frac{[B]}{[A]} = \frac{\alpha}{1-\alpha} = \exp\left(-\frac{\Delta H}{RT} + \frac{\Delta S}{R}\right),$$

$$\alpha(T) = \frac{K(T)}{1+K(T)} \quad \text{(A-4)}$$

where [A] and [B] are the concentrations of the two species.

(C) The Extended All-or-None Model Describing the Equilibrium of the Duplex, Hairpin, and Random Coil Conformations. The dissociation of the 8-, 12-, 16-, and 20-bp duplexes was described in terms of an extended all-or-none model involving duplex (ds), hairpin (hp), and random coil (rc) conformations. There is a monomolecular temperature-dependent equilibrium between the two forms of single strands with a distinct ΔH and ΔS; the hairpin is more stable at lower temperatures and the random coil predominates at higher temperatures. The thermodynamics of the duplex → single-stranded strand dissociation process is affected by this equilibrium between hairpins and random coils. The effect of the existence of the hairpin on the dissociation constant of the duplex is negligible if the T_m of the hairpin is far below the T_m of the duplex. The chemical reactions and equilibrium constants of the system are the following:

$$ds \leftrightarrow rc_1 + rc_2, \quad K_d(T) = \frac{[rc_1][rc_2]}{[ds]} = \exp\left(-\frac{\Delta H}{RT} + \frac{\Delta S}{R}\right),$$

$$hp_1 \leftrightarrow rc_1,$$

$$K_{hp_1}(T) = [rc_1]/[hp_1] = \exp\left(-\frac{\Delta H_{hp_1}}{RT} + \frac{\Delta S_{hp_1}}{R}\right),$$

$$hp_2 \leftrightarrow rc_2,$$

$$K_{hp_2}(T) = [rc_2]/[hp_2] = \exp\left(-\frac{\Delta H_{hp_2}}{RT} + \frac{\Delta S_{hp_2}}{R}\right) \quad \text{(A-5)}$$

where ds means the double-stranded species, rc_1 and rc_2 are the random coils, hp_1 and hp_2 are the hairpin conformations of the two complementary strands, K_d and K_{hp_i} ($i = 1, 2$) are the equilibrium constants of the dissociation of the duplex and of the melting of the hairpins, ΔH and ΔS are the molar enthalpy and entropy differences between the random coil and the duplex state, and ΔH_{hp_i} and ΔS_{hp_i} are the molar enthalpy and entropy differences between the random coil and hairpin of the ith strand. In our calculations we assumed that $\Delta H_{hp_1} = \Delta H_{hp_2}$ and $\Delta S_{hp_1} = \Delta S_{hp_2}$, that is, the thermal stabilities of the hairpins of the two complementary strands are the same; thus, $[rc_1] = [rc_2]$ and $[hp_1] = [hp_2]$. Using these equalities and omitting the indexes i referring to the two strands, we can define an extent of melting and an apparent dissociation constant by the following equations:

$$A(T) = \frac{K_d^*(T)}{c_0} = \frac{\alpha^2}{1-\alpha},$$

$$\alpha(T) = \frac{-A(T) + (A(T)^2 + 4A(T))^{1/2}}{2} \quad \text{(A-6)}$$

$$K_d^*(T) = \frac{[ss]^2}{[ds]} = \frac{([hp]+[rc])^2}{[ds]} = \frac{[rc]^2}{[ds]}\left(1 + \frac{[hp]^2}{[rc]^2} + 2\frac{[hp]}{[rc]}\right) = K_d(T)(1 + K_{hp}(T)^{-2} + 2K_{hp}(T)^{-1}) = \exp\left(-\frac{\Delta H}{RT} + \frac{\Delta S}{R}\right)\left[1 + 2\exp\left(\frac{\Delta H_{hp}}{RT} - \frac{\Delta S_{hp}}{R}\right) + \exp\left(\frac{2\Delta H_{hp}}{RT} - \frac{2\Delta S_{hp}}{R}\right)\right] = \exp\left(-\frac{\Delta H}{RT} + \frac{\Delta S}{R}\right)K_{cor}(T),$$

where ss refers to single strands either in the hp or in the rc conformation, α is the molar fraction of ss molecules, and c_0 is the duplex concentration if all the molecules are in the duplex state. $K_{cor}(T)$ is the correction factor for the apparent dissociation constant. $K_{cor}(T)$ was determined from melting experiments using the TMRh-labeled single strands of the duplexes. As we can see, K_d^*, the apparent dissociation constant of the duplex, and α, the extent-of-melting, can be expressed in terms of the temperature and the thermodynamic parameters of the duplex−random coil and hairpin-random coil transitions.

The Concentration Dependence of the T_m in the Extended All-or-None Model. We define T_m as the temperature where [ds] = [rc$_1$] = [rc$_2$] = [rc] (rc can mean either rc$_1$ or rc$_2$ and hp stands for either hp$_1$ or hp$_2$). We define c and c_0 as c = [ds] + [rc] and c_0 = [ds] + [rc] + [hp]. At $T = T_m$ where, according to our definitions, [ds] = [rc] = c/2 and [hp] = $c_0 - c$, the reaction equilibria are the following:

$$\frac{[rc]}{[hp]} = \frac{c/2}{c_0 - c} = \exp\left(-\frac{\Delta H_{hp}}{RT_m} + \frac{\Delta S_{hp}}{R}\right); \qquad \frac{[rc]^2}{[ds]} = c/2 = \exp\left(-\frac{\Delta H}{RT_m} + \frac{\Delta S}{R}\right) \quad \text{(A-7)}$$

Note that both c and T_m are unknown. If c_0 and the thermodynamic parameters ΔH, ΔS, ΔH_{hp}, and ΔS_{hp} of the reaction equilibria are all known, the above system of two equations can be solved for T_m and c. The second equation can also be written in the following form indicating clearly the concentration dependence of T_m:

$$1/T_m = -(R/\Delta H)\ln c + (\Delta S + R\ln 2)/\Delta H \quad \text{(A-8)}$$

Simulating Melting Curves with the Statistical Zipper Model. The melting of longer molecules is often not well-described by the all-or-none model. Longer duplex molecules undergo stepwise melting, and the reaction mixture may contain partially melted intermediates. A good discussion of the statistical mechanical models describing the melting of chain molecules can be found in the treatise (*16*). The zipper model (*16*) assumes that the molecules open up at the ends of the helix and the process of melting proceeds away from the ends similarly to the opening of a zipper; conformations containing internal loops are excluded. In our model we allow the molecule to open from both ends simultaneously. The $Z(N)$ partition function of the molecule N residues long is the following:

$$Z(N) = \sum_i \exp(-G_i/RT) \quad \text{(A-9)}$$

where R is the gas constant, T is the temperature in K, and G_i is the molar Gibbs free energy of the molecule in the ith conformation. The summation is taken over all possible conformations, i, allowed by the zipper model. $G_i = H_i - TS_i$, where H_i and S_i are the corresponding enthalpy and entropy of the conformation. $G_{coil} = 0$ is assumed for the coil state, and all bases are assumed to be equivalent in the coil state. A specific enthalpy change, $\Delta H_{j,bp}$, and a specific entropy change, $\Delta S_{j,bp}$, are assigned to the opening of the jth base pair of the sequence. Thus $G_{duplex} = -\sum_{j=1}^{N}(\Delta H_{j,bp} - T\Delta S_{j,bp})$ for the intact duplex. Sequence specificity can be taken into account by assigning different values of $\Delta H_{j,bp}$, and $\Delta S_{j,bp}$ for every base pair. A special concentration-dependent "nucleation parameter" can be assigned to the opening of the last intact base pair of the molecule. The total Gibbs free energy of a conformation is equal to the sum of the contributions of each base pair. If, for example, the first l base pairs are open and the last Nl base pairs are closed, then

$$G_i = G_{duplex} + \sum_{j=1}^{l}(\Delta H_{j,bp} - T\Delta S_{j,bp}) \quad \text{(A-10)}$$

The statistical weight, W_i, of the ith conformation is defined as $W_i = \exp(-G_i/RT)$, and the molecular fraction of a conformation is equal to $W_i/Z(N)$. Note that the molecular fraction of a conformation is temperature-dependent. The molecular fraction β of a class "U" of conformations is the sum of the statistical weights of the conformations belonging to "U" divided by the partition function:

$$\beta = \sum_{i\in U} W_i/Z(N) \quad \text{(A-11)}$$

In the simulation of the melting we assumed that the helix/coil state of the base pairs in a well-defined contiguous range (we will call this the "critical range") consisting of n base pairs (the "critical base pairs") determines the fluorescence signal of the molecule. Only base pairs near the labeling position are expected to affect the signal. The fluorescence signal of a conformation can have one of $n + 1$ possible different values, depending on how many bases belong to the coil segment existing at the fluorescently labeled end of the molecule. The apparent degree of melting of one molecule is k_i/n, where k_i is the number of critical base pairs in the coil segment at the labeled end of the molecule. The apparent extent-of-melting α of the mixture is calculated by the following sum:

$$\alpha = \sum_{i\in U} \frac{k_i}{n} W_i/Z(N) \quad \text{(A-12)}$$

where U represents the set of conformations in which the coil segment at the labeled end of the molecule contains at least one base pair of the critical range.

Experimental extent-of-melting curves can be approximated with simulated curves by varying the values of the energetic parameters $\Delta H_{j,bp}$ and $\Delta S_{j,bp}$ assigned to the opening of the individual base pairs and changing the position and

length of the critical region. In our simulations we set equal values for $\Delta H_{j,bp}$ for each internal base pair and varied only this common $\langle \Delta H_{bp} \rangle$ value. The entropy values of $\Delta S_{j,bp}$ were set to a uniform value of $\langle \Delta S_{bp} \rangle = 24$ cal/mol/K. The calculation of the partition functions and the molecular fractions was performed on a computer by using numerical techniques.

REFERENCES

1. Clegg, R. M., Murchie, A. I. H., Zechel, A., and Lilley, D. M. J. (1993) *Proc. Natl. Acad. Sci. U.S.A. 90*, 2994−2998.
2. Gohlke, C., Murchie, A. I. H., Lilley, D. M. J., and Clegg, R. M. (1994) *Proc. Natl. Acad. Sci. U.S.A. 91*, 11660−11664.
3. Murchie, A. I. H., Clegg, R. M., von Kitzing, E., Duckett, D. R., Diekmann, S., and Lilley, D. M. J. (1989) *Nature 341*, 763−766.
4. Clegg, R. M., Murchie, A. I. H., Zechel, A., Carlberg, C., Diekmann, S., and Lilley, D. M. J. (1992) *Biochemistry 31*, 4846−4856.
5. Clegg, R. M., Murchie, A. I. H., and Lilley, D. M. J. (1994) *Biophys. J. 66*, 99−109.
6. Cooper, J. P., and Hagerman, P. J. (1990) *Biochemistry 29*, 9261−9268.
7. Eis, P. S., and Millar, D. P. (1993) *Biochemistry 32*, 13852−13860.
8. Millar, D. P., and Fee, R. S. (1997) *Biophys. J. 72*, A6.
9. Yang, M., and Millar, D. P. (1996) *Biochemistry 35*, 7959−7967.
10. Cardullo, R. A., Agrawal, S., Flores, C., Zamecnik, P. C., and Wolf, D. E. (1988) *Proc. Natl. Acad. Sci. U.S.A. 85*, 8790−8794.
11. Parkhurst, K. M., and Parkhurst, L. J. (1993) *Biophys. J. 64*, A266.
12. Morrison, L. E., and Stols, L. M. (1993) *Biochemistry 32*, 3095−3104.
13. Xu, D., Evans, K. O., and Nordlund, T. M. (1994) *Biochemistry 33*, 9592−9599.
14. Parkhurst, K. M., and Parkhurst, L. J. (1995) *Biochemistry 34*, 285−292.
15. Breslauer, K. J., Frank, R., Blöcker, H., and Marky, L. A. (1986) *Proc. Natl. Acad. Sci. U.S.A. 83*, 3746−3750.
16. Poland, D., and Scheraga, H. A. (1970) *Theory of Helix-Coil Transitions in Biopolymers*, Academic Press, New York.
17. Vámosi, G., Gohlke, C., and Clegg, R. M. (1996) *Biophys. J. 71*, 972−994.
18. Haasnoot, C. A., den Hartog, J. H. J., de Rooij, J. F. M., van Boom, J. H., and Altona, A. (1980) *Nucleic Acids Res. 8*, 169−181.
19. Orbons, L. P., van der Marel, G. A., van Boom, J. H., and Altona, C. (1986) *Nucleic Acids Res. 14*, 4187−4196.
20. Rinkel, L. J., van der Marel, G. A., van Boom, J. H., and Altona, C. (1987) *Eur. J. Biochem. 166*, 87−101.
21. Pieters, J. M., Mellema, J. R., van den Elst, H., van der Marel, G. A., van Boom, J. H., and Altona, C. (1989) *Biopolymers 28*, 717−740.
22. Antao, V. P., Lai, S. Y., and Tinoco, I., Jr. (1991) *Nucleic Acids Res. 19*, 5901−5905.
23. Antao, V. P., and Tinoco, I., Jr. (1992) *Nucleic Acids Res. 20*, 819−824.
24. Avizonis, D. Z., and Kearns, D. R. (1995) *Biopolymers 35*, 187−200.
25. Varani, G. (1995) *Ann. Rev. Biophys. Biomol. Struct. 24*, 379−404.
26. Beaucage, S. L., and Caruthers, M. H. (1981) *Tetrahedron Lett. 22*, 1859−1862.
27. Connolly, B. A. (1987) *Nucleic Acids Res. 15*, 3131−3139.
28. Lakowicz, J. R. (1983) *Principles of Fluorescence Spectroscopy*, Plenum Press, New York.
29. Gratton, E., Jameson, D. M., Rosato, N., and Weber, G. (1984) *Rev. Sci. Instrum. 55*, 486−494.
30. Jameson, D. M., Gratton, E., and Hall, R. D. (1984) *Appl. Spectrosc. Rev. 20*, 55−106.
31. Piston, D. W., Marriott, G., Radivoyevich, T., Clegg, R. M., Jovin, T. M., and Gratton, E. (1989) *Rev. Sci. Instrum. 60*, 2596−2600.
32. Förster, T. (1948) *Ann. Phys. 2*, 55−75.
33. Förster, T. (1951) *Fluoreszenz Organischer Verbindungen*, Vandenhoeck & Ruprecht, Göttingen, Germany.
34. Clegg, R. M. (1996) in *Fluorescence Imaging Spectroscopy and Microscopy* (Wang, X. F., and Herman, B., Eds.) pp 179−252, John Wiley & Sons, Inc., New York.
35. Dale, R. E., Eisinger, J., and Blumberg, W. E. (1979) *Biophys. J. 26*, 161−194.
36. Hirao, I., Kawai, G., Yoshizawa, S., Nishimura, Y., Ishido, Y., Watanabe, K., and Miura, K. (1994) *Nucleic Acids Res. 22*, 576−582.
37. Gohlke, C. (1994) Masters Thesis, Georg-August Universität, Göttingen, Germany.
38. Gralla, J., and Crothers, D. M. (1973) *J. Mol. Biol. 73*, 497−511.
39. Stühmeier, F., Lilley, D. M. J., and Clegg, R. M. (1997) *Biochemistry 36*, 13539−13555.

BI9727601